Numerical renormalization group calculations of the magnetization of Kondo impurities with and without uniaxial anisotropy

Martin Höck* and Jürgen Schnack†
Fakultät für Physik, Universität Bielefeld, Postfach 100131, D-33501 Bielefeld, Germany
(Received 6 February 2013; published 9 May 2013)

We study a Kondo impurity model with additional uniaxial anisotropy D in a nonzero magnetic field B using the numerical renormalization group (NRG). The ratio g_e/g_S of electron and impurity g factor is regarded as a free parameter and, in particular, the special cases of a "local" ($g_e = 0$) and "bulk" ($g_e = g_S$) field are considered. For a bulk field, the relationship between the impurity magnetization $\mathcal{M}$ and the impurity contribution to the magnetization M_{imp} is investigated and it is shown that $\mathcal{M}$ and M_{imp} are proportional to each other for fixed coupling strength. Furthermore, we find that the g-factor ratio effectively rescales the magnetic field argument of the zero-temperature impurity magnetization. In case of an impurity with $D = 0$ and $g_e = g_S$, it is demonstrated that at zero temperature $\mathcal{M}(B)$, unlike $M_{\text{imp}}(B)$, does *not* display universal behavior. With additional "easy-axis" anisotropy, the impurity magnetization is "stabilized" at a D-dependent value for $k_BT \ll g_S\mu_B B \ll |D|$ and, for nonzero temperature, is well described by a shifted and rescaled Brillouin function on energy scales that are small compared to $|D|$. In the case of "hard-axis" anisotropy, the magnetization curves can feature steps which are due to field-induced pseudo-spin-$\frac{1}{2}$ Kondo effects. For large hard-axis anisotropy and a local field, these screening effects are described by an exchange-anisotropic spin-$\frac{1}{2}$ Kondo model with an additional scattering term that is spin dependent (in contrast to ordinary potential scattering). In accordance with the observed step widths, this effective model predicts a decrease of the Kondo temperature with every further step that occurs upon increasing the field. Our study is motivated by the question as to how the magnetic properties of a deposited magnetic molecule are modified by the interaction with a nonmagnetic metallic surface.

DOI: 10.1103/PhysRevB.87.184408 PACS number(s): 73.20.Hb, 75.30.Cr, 75.30.Gw, 75.50.Xx

I. INTRODUCTION

Magnetic molecules offer the prospect of encoding and storing information in their magnetic state. The latter point applies, in particular, to bistable molecules such as single-molecule magnets (SMMs).[1–4] The possibility to store, e.g., one bit of information in the state of a single molecule would constitute an enormous miniaturization and could lead to data storage technologies with significantly increased areal density.[5] However, to make a (potentially elusive) technological application feasible, the molecules need to be individually addressable so that their magnetic state can be probed and manipulated on a molecule-by-molecule basis. In the last years, there has been an increasing interest in the question as to whether this functionality can be achieved by a controlled deposition of magnetic molecules on suitable substrates.[5–8] While such an approach might solve the problem of addressability, it can introduce new complications due to interactions between the molecules and the surface. Depending on details such as the molecule's ligands, the presence of an additional decoupling layer, and, of course, the characteristics of the surface, the interaction with the substrate might alter the magnetic properties of the molecule in an important (and possibly adverse) way. Thus, even if the magnetic response of the isolated molecule is well understood (e.g., through a description by a suitable spin model[9]), its magnetic properties in contact with the surface have to be reinvestigated.

In this paper, we study a single-channel Kondo impurity model with nonzero magnetic field and additional uniaxial anisotropy $D(\underset{\sim}{S}^z)^2$ for the impurity spin operator $\underset{\sim}{\boldsymbol{S}}$. Such an anisotropy term {along with transverse anisotropy $E[(\underset{\sim}{S}^x)^2 - (\underset{\sim}{S}^y)^2]$} is a common part of a pure spin model for the description of isolated magnetic molecules (in particular, for representing SMMs).[9] The quantum impurity model is intended to serve as a minimal representation of an anisotropic magnetic molecule on a nonmagnetic metallic substrate and, with transverse anisotropy E, has already been used to describe SMMs interacting with metallic electrodes.[10–12] Furthermore, it has been found that the above uniaxial and transverse anisotropy terms are also appropriate to model the surface-induced anisotropy of a single magnetic atom on a metallic substrate with a decoupling layer.[13–15] To investigate how the interaction with the electrons affects the magnetic properties of the impurity, we carry out numerical renormalization group[16–18] (NRG) calculations and focus on the magnetic field dependence of the impurity magnetization.

Regarding the experimental situation, the magnetic moment of deposited molecules (or atoms)[15] can be measured using methods such as x-ray magnetic circular dichroism (XMCD).[7,19–27] XMCD is an element-specific technique of high sensitivity based on the absorption of circularly polarized x rays and can be used to obtain an ensemble-averaged result for the magnetic-field-dependent molecule magnetization.[28–30] In principle, it is also possible to extract information about different contributions to the observed magnetic moment (such as the orbital and spin contribution) from the XMCD data using, e.g., sum rules.[7,21,22,24,27] In the last years, magnetization curves of magnetic atoms on nonmagnetic metallic surfaces could also be recorded using spin-polarized scanning tunneling spectroscopy (SP-STS).[15,31–35] In contrast to XMCD, this method provides a time average of the field-dependent magnetic moment of a single atom. It has been demonstrated that SP-STS can also be applied to (suitable) deposited magnetic molecules.[36–38]

The static magnetization of Kondo impurity models (including related models such as the single-impurity Anderson model) has been investigated by a number of techniques. Among these are Green's-function methods,[39,40] the Bethe ansatz,[41–52] and NRG (Refs. 53–55) (including density matrix based extensions). By now, there are also several studies of the time dependence of the magnetization in nonequilibrium situations (e.g., after a quantum quench or with a nonzero voltage bias).[56–60] In particular, nonequilibrium spin dynamics of impurity models can be investigated by using a generalization of NRG called time-dependent NRG (TD-NRG).[12,61,62]

This paper extends existing NRG results for the Kondo model with uniaxial anisotropy[63] to the case of nonzero magnetic field. The system with nonzero field (with a focus on the properties of spectral functions) has been previously studied in Refs. 64 and 65. Furthermore, magnetization curves for isotropic Kondo impurities and for a Kondo impurity featuring both longitudinal and transverse anisotropy have been calculated in Ref. 55. We would like to stress, however, that our investigation places emphasis on different aspects of the problem and is thus complementary to Ref. 55.

The remainder of this paper is organized as follows. In Sec. II, the quantum impurity model is introduced and transformed to a representation that is suitable for further numerical treatment. Section III provides information about our use of the NRG method and contains definitions of the considered observables. In Sec. IV, we study the magnetic field dependence of the impurity magnetization and the impurity contribution to the magnetization for an isotropic system (i.e., with anisotropy parameter $D = 0$) and analyze the relation between both quantities. After an investigation of the Kondo model with additional "easy-axis" anisotropy ($D < 0$) in Sec. V, the case of "hard-axis" anisotropy ($D > 0$) is considered in Sec. VI. In order to describe the field-induced pseudo-spin-$\frac{1}{2}$ Kondo effects that are observed in the magnetization curves for large hard-axis anisotropy, an effective model is derived and its properties are studied. We conclude this paper with a summary of the results in Sec. VII. Appendix A contains a brief description of the technical details of a NRG calculation with nonzero magnetic coupling of the conduction electrons. The remaining Appendices are concerned with the coupling strength dependence of the magnetization for $D = 0$ (Appendix B), the effect of a nonzero magnetic coupling of the conduction electrons on the impurity magnetization curves (Appendix C), and certain technical aspects relevant to the study of the effective model (Appendix D).

II. MODEL

A. Hamiltonian

In this work, we study a Hamilton operator $\underset{\sim}{H}$ consisting of three parts:

$$\underset{\sim}{H} = \underset{\sim}{H}_{\text{electrons}} + \underset{\sim}{H}_{\text{coupling}} + \underset{\sim}{H}_{\text{impurity}}. \tag{1}$$

The first term $\underset{\sim}{H}_{\text{electrons}}$ represents noninteracting tight-binding electrons whose hopping between two sites i and j of a periodic lattice with L sites is described by the corresponding hopping parameter t_{ij}:

$$\underset{\sim}{H}_{\text{electrons}} = \sum_{i\neq j,\,\sigma} t_{ij}\underset{\sim}{d}^{\dagger}_{i\sigma}\underset{\sim}{d}_{j\sigma} + g_e\mu_B B\underset{\sim}{\mathcal{S}}^{z}. \tag{2}$$

Here, $\underset{\sim}{d}^{(\dagger)}_{i\sigma}$ is a destruction (creation) operator for an electron with spin projection $\sigma = \pm\frac{1}{2} \mathrel{\widehat{=}} \uparrow/\downarrow$ at lattice site i. The effect of an external magnetic field B is taken into account by a Zeeman term with electron g factor g_e, Bohr magneton μ_B, and the z component of the total spin of the electrons,

$$\underset{\sim}{\mathcal{S}}^{z} = \frac{1}{2}\sum_i (\underset{\sim}{n}_{i\uparrow} - \underset{\sim}{n}_{i\downarrow}), \tag{3}$$

with $\underset{\sim}{n}_{i\sigma} = \underset{\sim}{d}^{\dagger}_{i\sigma}\underset{\sim}{d}_{i\sigma}$. Using a discrete Fourier transformation $\underset{\sim}{c}^{\dagger}_{\boldsymbol{k}\sigma} = (1/\sqrt{L})\sum_j e^{i\boldsymbol{k}\cdot\boldsymbol{R}_j}\underset{\sim}{d}^{\dagger}_{j\sigma}$, Hamiltonian (2) can be equivalently written in the more common form

$$\underset{\sim}{H}_{\text{electrons}} = \sum_{\boldsymbol{k},\sigma} \underbrace{(\varepsilon_{\boldsymbol{k}} + \sigma g_e\mu_B B)}_{=\varepsilon_{\boldsymbol{k}\sigma}(B)} \underset{\sim}{c}^{\dagger}_{\boldsymbol{k}\sigma}\underset{\sim}{c}_{\boldsymbol{k}\sigma}, \tag{4}$$

with a dispersion relation $\varepsilon_{\boldsymbol{k}\sigma}(B)$, assigning an energy ε to a wave vector $\boldsymbol{k}$, that now depends on spin projection and magnetic field. In general, the spin-independent dispersion relation $\varepsilon_{\boldsymbol{k}}$ is anisotropic in $\boldsymbol{k}$ space.

For the interaction term in Eq. (1), we use a standard isotropic Kondo coupling,

$$\underset{\sim}{H}_{\text{coupling}} = J\,\underset{\sim}{\boldsymbol{S}}\cdot\underset{\sim}{\boldsymbol{s}}_0, \tag{5}$$

and assume that the impurity spin $\underset{\sim}{\boldsymbol{S}}$ couples antiferromagnetically ($J > 0$) to the electronic spin at the origin, which is given by $\underset{\sim}{\boldsymbol{s}}_0 = (1/2L)\sum_{\boldsymbol{k},\boldsymbol{k}',\mu,\nu}\underset{\sim}{c}^{\dagger}_{\boldsymbol{k}\mu}\boldsymbol{\sigma}_{\mu\nu}\underset{\sim}{c}_{\boldsymbol{k}'\nu}$ with the vector of Pauli matrices $\boldsymbol{\sigma}$.

Finally, the impurity part of Hamiltonian (1) represents a localized spin with quantum number S which couples to the external magnetic field with g factor g_S and possesses an additional uniaxial anisotropy D:

$$\underset{\sim}{H}_{\text{impurity}} = D(\underset{\sim}{S}^{z})^2 + g_S\mu_B B\underset{\sim}{S}^{z}. \tag{6}$$

With the chosen convention, the impurity spin has an easy axis for $D < 0$ and a hard axis or an "easy plane" for $D > 0$. A further transverse anisotropy $E[(\underset{\sim}{S}^{x})^2 - (\underset{\sim}{S}^{y})^2]$ is *not* considered in this paper. $\underset{\sim}{H}_{\text{impurity}}$ can be seen as a minimal representation of a magnetic molecule with a single magnetic center or as a "giant spin approximation" for an SMM.[9,66]

Hamiltonian (1) corresponds to an exchange-isotropic single-channel Kondo impurity model with additional uniaxial anisotropy and nonzero external magnetic field. The special choices $g_e = 0$ and g_S for the electron g factor are referred to as a "local" and "bulk" magnetic field, respectively. Regarding the modeling of a deposited magnetic molecule, it has to be emphasized that Hamiltonian (1) suffers from a number of simplifications. For example, there is no orbital contribution to the magnetism, and no charge fluctuations between molecule and surface are possible. In this paper, we only consider the effect of the Kondo coupling on the magnetic properties of the impurity spin.

B. Transformation to an energy representation

In order to treat Hamiltonian (1) using NRG, $\underset{\sim}{H}_{\text{electrons}}$ and $\underset{\sim}{H}_{\text{coupling}}$ are expressed via a continuous energy representation for the electronic degrees of freedom. To this end, we first take a standard continuum limit in $\boldsymbol{k}$ space (i.e., we consider a lattice of dimension d with $L \gg 1$).[17] By adapting the corresponding expression for the two-impurity Kondo model from Ref. 67 to the single-impurity case (see also Ref. 68), we then define those states with energy ε to which the localized spin *directly* couples:

$$\underset{\sim}{a}_{\varepsilon\mu} = \frac{1}{\sqrt{(2\pi)^d \rho(\varepsilon - \mu h)}} \int d\boldsymbol{k}\, \delta(\varepsilon - \varepsilon_\mu(\boldsymbol{k}, B))\, \underset{\sim}{c}_{\boldsymbol{k}\mu}, \qquad (7)$$

where we have introduced the abbreviation $h = g_e \mu_B B$ and the density of states (DOS) per spin projection and lattice site $\rho(\varepsilon) = (1/L)\sum_{\boldsymbol{k}} \delta(\varepsilon - \varepsilon_{\boldsymbol{k}})$. Denoting the half-width of the conduction band by W and removing all electronic states that decouple from the impurity, the desired continuous energy representation of Hamiltonian (1) is obtained:

$$\begin{aligned} \underset{\sim}{H} \to & \sum_\mu \int_{-W+\mu h}^{W+\mu h} d\varepsilon\, \varepsilon\, \underset{\sim}{a}^\dagger_{\varepsilon\mu} \underset{\sim}{a}_{\varepsilon\mu} \\ & + J \underset{\sim}{\boldsymbol{S}} \cdot \sum_{\mu,\nu} \left(\int_{-W+\mu h}^{W+\mu h} d\varepsilon \sqrt{\rho(\varepsilon - \mu h)}\, \underset{\sim}{a}^\dagger_{\varepsilon\mu} \right) \frac{\boldsymbol{\sigma}_{\mu\nu}}{2} \\ & \times \left(\int_{-W+\nu h}^{W+\nu h} d\varepsilon' \sqrt{\rho(\varepsilon' - \nu h)}\, \underset{\sim}{a}_{\varepsilon'\nu} \right) + \underset{\sim}{H}_{\text{impurity}}. \end{aligned} \qquad (8)$$

For $h = 0$, i.e., for $B = 0$ or $g_e = 0$, Eq. (8) reduces to the well-known expression for the energy representation of the Kondo model.[69] In the following, we consider the case of a constant DOS: $\rho(\varepsilon) = 1/2W = \rho$.

III. METHOD AND OBSERVABLES

A. Method: NRG

Approximate eigenvalues and eigenvectors of Hamiltonian (8) for the calculation of impurity properties can be obtained with the numerical renormalization group.[16–18] However, the procedure leading to the parameters of the Wilson chain has to be slightly modified if $h \neq 0$ (see Appendix A for a brief discussion of the required changes).

Both a nonzero magnetic field and an additional uniaxial anisotropy break the full SU(2) symmetry in spin space of Hamiltonian (1). For this reason, we label eigenstates of $\underset{\sim}{H}$ only with the charge quantum number Q and the magnetic quantum number S^z_{total} of the z component of the total spin (note that with additional transverse anisotropy or a magnetic field applied in some different direction S^z_{total} would not be a good quantum number). Except for one example in Appendix D, all NRG calculations are carried out using the improved discretization scheme proposed by Žitko and Pruschke[70,71] with averaging over four z values that are equidistantly spaced on the interval $(0,1]$. The Hamiltonians describing the truncated Wilson chain are always rescaled by employing Wilson's analytical solution for the hopping parameters for the case of the standard discretization with $z = 1$.[16,18] Observables are computed using only those states that are kept after truncation and results are averaged over even and odd sites of the Wilson chain according to the prescription of Ref. 18. We use a discretization parameter $\Lambda = 3$, a dimensionless inverse temperature $\bar{\beta} = 0.7$, and a fixed number of kept states of the order of 5000 to achieve convergence for all considered observables within the resolution of the presented plots. Nevertheless, at $\Lambda > 1$ there might still be slight systematic deviations for nonzero temperature, which can for example be demonstrated by setting $J = 0$ and comparing the NRG results with the analytical solution for a free spin. It is necessary to perform a separate NRG calculation for each value of the magnetic field. If curves are shown in a plot, they are thus the result of a spline interpolation through the numerically obtained data points.

Calculation of the impurity magnetization [defined in Eq. (9)] requires matrix elements of $\underset{\sim}{S}^z$ with respect to the eigenstates of the truncated Wilson chains. In each step of the iterative diagonalization of the Wilson chain, we therefore set up a matrix representation $\mathcal{P}(\underset{\sim}{S}^z)$ with respect to the current product basis by using the matrix elements from the previous step. Having obtained the matrix of eigenvectors $\mathcal{U}$, $\mathcal{P}(\underset{\sim}{S}^z)$ is then transformed to the eigenbasis of the truncated Wilson chain according to $\mathcal{E}(\underset{\sim}{S}^z) = \mathcal{U}^\dagger \mathcal{P}(\underset{\sim}{S}^z)\mathcal{U}$.

A NRG calculation gives thermodynamic expectation values for a discrete set of nonzero temperatures, which are chosen (by specifying $\bar{\beta}$) in such a way as to sample the "good" part of the finite-size energy spectrum in each step of the iterative diagonalization.[18] For this reason, it is not possible to truly consider the case $T = 0$. If the temperature is referred to as "negligible" or "approximately zero" in the remainder of this paper, it is therefore always meant that the thermal energy is smaller by orders of magnitude compared to all other relevant energy scales so that no significant temperature-related effects are observable in the presented results.

B. Observables

In our calculations, we focus on the impurity magnetization which is defined as the thermodynamic expectation value of the impurity magnetization operator

$$\mathcal{M}(T,B) = -\left\langle \frac{\partial \underset{\sim}{H}_{\text{impurity}}}{\partial B} \right\rangle = -g_S \mu_B \langle \underset{\sim}{S}^z \rangle. \qquad (9)$$

Furthermore, we consider the impurity contribution to the entropy, magnetization, and magnetic susceptibility. The impurity contribution to some quantity $\mathcal{O}$ is defined in the usual way:[18]

$$\mathcal{O}_{\text{imp}} = \mathcal{O}^{\text{with impurity}}_{\text{total}} - \mathcal{O}^{\text{w/o impurity}}_{\text{total}}. \qquad (10)$$

The observable $\mathcal{O}^{\text{w/o impurity}}_{\text{total}}$ for the system without impurity is also calculated using NRG by removing the impurity part from the Wilson chain. For the entropy $S(T,B)$, the magnetization $M(T,B)$, and the susceptibility $\chi(T,B)$, we use the standard definitions $S(T,B) = -\partial\Omega(T,B)/\partial T$, $M(T,B) = -\partial\Omega(T,B)/\partial B$, and $\chi(T,B) = \partial M(T,B)/\partial B$, with $\Omega(T,B)$ being the grand-canonical potential. According to the definitions (3), (9), and (10), the impurity contribution to the

magnetization M_{imp} can be written as

$$M_{\text{imp}} = \mathcal{M} - g_e \mu_B (\langle \underset{\sim}{\mathcal{S}}^z \rangle^{\text{with imp}} - \langle \underset{\sim}{\mathcal{S}}^z \rangle^{\text{w/o imp}}). \quad (11)$$

If the electron g factor is zero or if impurity and electrons decouple (which happens for $J \to 0$ or $T \to \infty$), we thus have the special case $M_{\text{imp}}(T,B) = \mathcal{M}(T,B)$. In the grand-canonical calculations, the chemical potential is assumed to be zero. For a symmetric DOS, $\rho(\varepsilon) = \rho(-\varepsilon)$, the free-electron band is thus on average half-filled for arbitrary magnetic field and temperature.

IV. IMPURITIES WITH $D = 0$

Let us first consider the case of an isotropic impurity with $D = 0$ in Hamiltonian (6) and study the impurity contribution to the magnetization M_{imp} and the impurity magnetization $\mathcal{M}$, both as a function of temperature and magnetic field. For the moment, we are only concerned with the special case of equal g factors of impurity and electrons (corresponding to a bulk magnetic field). Recalling the motivation given in the introduction, $\mathcal{M}$ as the expectation value of the impurity magnetization operator should be the observable that is more closely related to experimental magnetization data obtained by methods such as XMCD.

A. Field dependence of the magnetization

In case of the Kondo model with $D = 0$, $g_e = g_S$, and arbitrary impurity spin S, the Bethe ansatz (BA) allows for the derivation of a closed expression for the impurity contribution to the magnetization at zero temperature.[41–44,46,47] In the scaling regime,[47] "bare" parameters of the model can be absorbed into a certain energy scale $k_B T_H$ so that the field dependence of $M_{\text{imp}}(T = 0)$ is described by a universal function $f_S(x)$ [see Eq. (5.1.33) of Ref. 46], with x being the rescaled magnetic field: $x = g_S \mu_B B / k_B T_H$. For each value of S, the energy scale $k_B T_H$ is chosen in such a way that the asymptotic high-field (i.e., $g_S \mu_B B \gg k_B T_H$) expansion of $f_S(x)$ does not contain terms of order $1/\ln^2(g_S \mu_B B / k_B T_H)$.[47,72] In case of impurity spin $S = \frac{1}{2}$, we adopt the convention of Ref. 46 according to which the Kondo temperature T_K is identified with the strong coupling scale (as opposed to the high-temperature scale)[47] and defined as

$$\frac{\chi_{\text{imp}}(T = 0, B = 0)}{(g_S \mu_B)^2} = \frac{1}{2\pi\, k_B T_K}. \quad (12)$$

The relation between T_H and T_K for $S = \frac{1}{2}$ is then given by[46]

$$T_H = \sqrt{\frac{2\pi}{e}}\, T_K. \quad (13)$$

Note that in the remainder of this paper, results for the energy scales $k_B T_H$ and $k_B T_K$ always refer to either the corresponding situation with $D = 0$ or a comparable situation with $D = 0$.

In Fig. 1, we plot the universal BA solution for $M_{\text{imp}}(T = 0)$ for three different impurity spins $S = \frac{1}{2}$, 1, and $\frac{3}{2}$.[73] $f_S(x)$ is a strictly monotonically increasing function of x and approaches the saturation magnetization of a free spin $g_S \mu_B S$ for $x \to \infty$ with slowly decaying logarithmic corrections.[46,47,72] The behavior in the limit $x \to 0$ depends on the value of S: In case

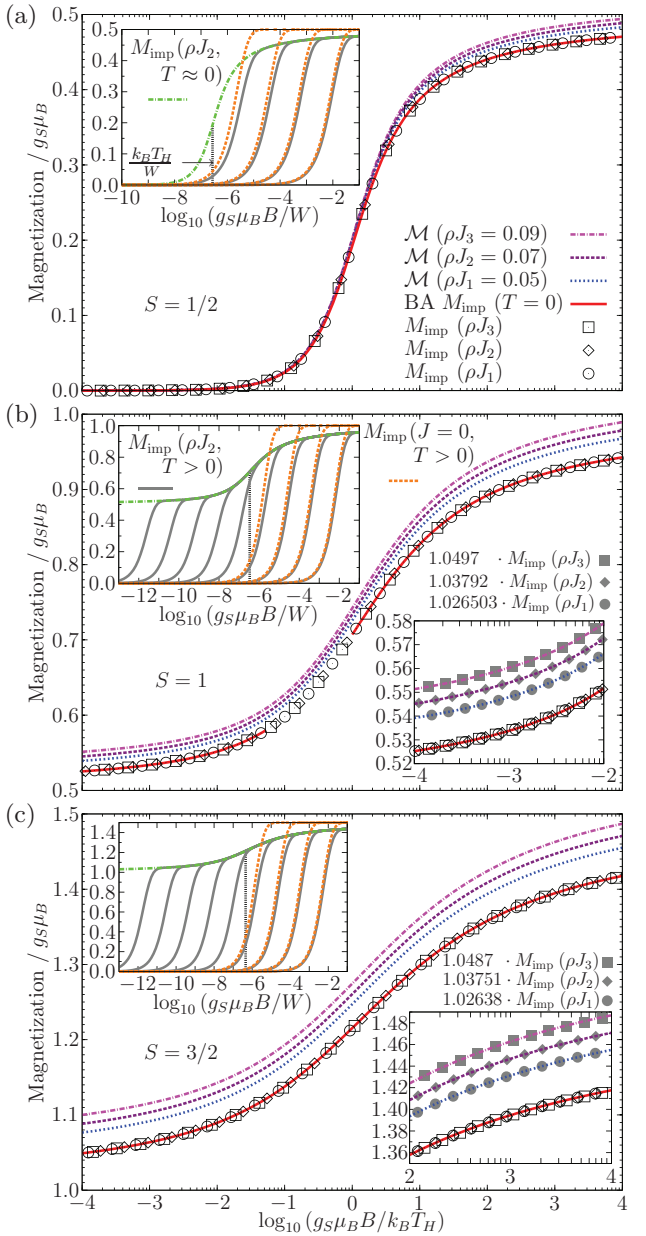

FIG. 1. (Color online) Main plots: Impurity contribution to the magnetization M_{imp} and impurity magnetization $\mathcal{M}$ as a function of magnetic field for $g_e = g_S$, three different couplings ρJ, and for impurity spin (a) $S = \frac{1}{2}$, (b) $S = 1$, and (c) $S = \frac{3}{2}$. The temperature is $k_B T/W \approx 1.54 \times 10^{-15} \approx 0$ and the field is rescaled using $k_B T_H$. In case of $S = 1$, part of the universal BA solution for $M_{\text{imp}}(x, T = 0)$ is missing in the regime $g_S \mu_B B \lesssim k_B T_H$ (Ref. 73). Upper left insets show NRG results for $M_{\text{imp}}(B)$ at $T \approx 0$ and finite temperature as a function of magnetic field, now expressed in units of W. $M_{\text{imp}}(B)$ for $J = 0$ is also computed using NRG and resembles the magnetization of the free spin (Ref. 74). Thermal energies increase from left to right and range from $1.79 \times 10^{-6} W$ [(a)] or $1.95 \times 10^{-12} W$ [(b) and (c)] to $6.79 \times 10^{-3} W$. Results for adjacent temperatures are calculated using truncated Wilson chains whose lengths differ by five lattice sites. Lower right insets show a closeup of the magnetization curves for (b) low fields and (c) high fields along with data points for M_{imp} that are multiplied by a coupling-dependent constant $\gtrsim 1$.

TABLE I. Approximate values of $k_B T_H/W$ as used in Fig. 1, obtained by fitting the universal Bethe ansatz solution for $M_{\rm imp}(x, T=0)$, and proportionality factors $\alpha(\rho J)$ relating $\mathcal{M}$ and $M_{\rm imp}$ according to Eq. (15). The results for α have been averaged over magnetic fields $g_S\mu_B B/W \in [10^{-13}, 10^{-1}]$ for $k_B T/W \approx 1.54 \times 10^{-15} \approx 0$. Numbers in parentheses give the corresponding standard deviation for the last decimal place. For Zeeman energies close to the band edge (i.e., for $g_S\mu_B B \lesssim W$), which have not been considered for the average, α noticeably decreases (increases) for $S = \frac{1}{2}$ ($S = 1, \frac{3}{2}$).

	$S=\frac{1}{2}$		$S=1$		$S=\frac{3}{2}$	
ρJ	$k_B T_H/W$	α	$k_B T_H/W$	α	$k_B T_H/W$	α
0.05	7.29×10^{-10}	1.02659(1)	8.49×10^{-10}	1.026503(7)	1.05×10^{-9}	1.02638(2)
0.07	2.74×10^{-7}	1.03822(2)	3.39×10^{-7}	1.03792(3)	4.55×10^{-7}	1.03751(6)
0.09	7.72×10^{-6}	1.05048(3)	1.02×10^{-5}	1.04970(8)	1.51×10^{-5}	1.0487(2)

of $S = \frac{1}{2}$, $f_{1/2}(x) \propto x$ for small x, whereas for $S \geqslant 1$ the function $f_S(x)$ goes to the saturation magnetization of a reduced spin with $S - \frac{1}{2}$, again with logarithmic corrections.[46,47,72] This low-field behavior mirrors the underscreened Kondo effect which, for vanishing magnetic field, reduces the impurity spin S to a residual spin $S - \frac{1}{2}$ in the limit $T/T_K \ll 1$.[75,76] The magnetic properties of the impurity are furthermore markedly different from that of a free spin as the magnetization of a free spin at $T = 0$ saturates for any positive magnetic field.

Using NRG, we have calculated $M_{\rm imp}(B, T \approx 0)$ for several values of the coupling strength ρJ and have fitted the obtained curves to the respective universal BA curve by employing T_H as a fit parameter (see Fig. 1). The nice agreement with the BA solution demonstrates the universal field dependence that $M_{\rm imp}$ displays for small ρJ and allows us to reliably determine the value of T_H for all considered impurity spins. However, note that for very large magnetic fields (i.e., for $g_S\mu_B B \lesssim W$), we leave the scaling regime and the rescaled $M_{\rm imp}$ curves, as calculated by NRG, start to drop below the universal BA curves (this is not shown in Fig. 1). The determined approximate values of $k_B T_H/W$ are given in Table I. We find that the fitted values of T_H increase with the impurity spin for fixed coupling strength and, furthermore, that the relative deviation between the results for different S decreases when ρJ is reduced. However, even for the smallest considered coupling strength ($\rho J = 0.05$), the values of T_H for $S = \frac{1}{2}$ and $S = \frac{3}{2}$ still deviate by about 44%. According to Eqs. (12) and (13), the values of T_H for $S = \frac{1}{2}$ reported in Table I correspond to the following Kondo temperatures: $k_B T_K/W \approx 4.79 \times 10^{-10}$ ($\rho J = 0.05$), 1.80×10^{-7} (0.07), and 5.08×10^{-6} (0.09). For comparison, the standard estimate for the Kondo temperature[16,17]

$$k_B T_K'/W \approx \sqrt{\rho J}\exp(-1/\rho J) \tag{14}$$

gives $k_B T_K'/W \approx 4.61 \times 10^{-10}$ ($\rho J = 0.05$), 1.65×10^{-7} (0.07), and 4.48×10^{-6} (0.09). As a further check, we have determined the Kondo temperature for $S = \frac{1}{2}$ and $\rho J = 0.07$ by fitting the zero-field BA solution for the impurity contribution to the susceptibility from Ref. 46 and the impurity contribution to the entropy from Ref. 77 [the specified low-temperature limit of the impurity contribution to the specific heat shows that their definition of T_K corresponds to Eq. (12)]. In both cases, a value of $k_B T_K/W \approx 1.79 \times 10^{-7}$ is obtained, which is quite similar to the one following from Table I.

The upper left insets of Fig. 1 show finite-temperature NRG results for $M_{\rm imp}(T, B)$ with a coupling strength $\rho J = 0.07$. As a reference point, we replot the zero-temperature magnetization curves that cross over to the strong coupling regime in the vicinity of $g_S\mu_B B \approx k_B T_H$. As long as the thermal energy is small compared to the Zeeman energy, the magnetization always closely follows the respective zero-temperature curve. On the other hand, if the thermal energy is not negligibly small compared to the Zeeman energy, we have to distinguish between complete screening and underscreening of the impurity spin. For $S \geqslant 1$, nonzero temperature is always important as it also affects the residual spin. On the energy scale $g_S\mu_B B \approx k_B T$, there is a swift drop of $M_{\rm imp}(B)$ that is eventually followed by a linear decay for small fields $g_S\mu_B B \ll k_B T$. In the special case $S = \frac{1}{2}$, however, nonzero temperature has little effect if $T \ll T_K$ and the magnetization already displays a linear dependence on the magnetic field for $g_S\mu_B B \approx k_B T$ due to the Kondo screening. In the upper left insets of Fig. 1 we also compare the results for $M_{\rm imp}(T, B)$ with NRG calculations for vanishing coupling $J = 0$.[74] At high temperatures (compared to T_H), the impurity spin is progressively decoupled from the electronic system and becomes asymptotically free so that its magnetization resembles the result for $J = 0$ more closely.

In addition to the impurity contribution to the magnetization $M_{\rm imp}$, we also plot the impurity magnetization $\mathcal{M}(B)$ for the same values of the coupling ρJ and negligible temperature in Fig. 1. The magnetic field is again rescaled by $k_B T_H$ using the values from Table I. We find that $\mathcal{M}$ and $M_{\rm imp}$ differ for all considered magnetic fields with $\mathcal{M}(B)$ being larger than $M_{\rm imp}(B)$ for given B. According to Eq. (11), this means that the magnetization of the conduction electrons is reduced due to the interaction with the impurity spin. Upon decreasing ρJ at constant rescaled field x, we observe that the impurity magnetization becomes smaller and thus approaches the universal curve for $M_{\rm imp}(x)$. A comparison of the NRG results for $\mathcal{M}$ and $M_{\rm imp}$ shows that both quantities are proportional to each other *for fixed coupling strength* ρJ, i.e.,

$$\mathcal{M}(B, T \approx 0) = \alpha(\rho J)\, M_{\rm imp}(B, T \approx 0)\,, \tag{15}$$

with a proportionality factor $\alpha > 1$ that depends on ρJ [see Table I for a list of the calculated values of $\alpha(\rho J)$]. With the accuracy indicated in Table I, relation (15) holds for Zeeman energies that are small compared to the half-bandwidth W. It is illustrated for the case of small magnetic fields (for $S = 1$) and large magnetic fields (for $S = \frac{3}{2}$) in the lower right insets

of Fig. 1. While the obtained values for $\alpha(\rho J)$ decrease with increasing impurity spin S, the values for different S differ by less than 0.2% according to Table I. Since impurity and electrons progressively decouple at high temperatures, we expect α to be temperature dependent with $\alpha \to 1$ for $k_B T/W \gg 1$ [cf. Eq. (11)]. The results presented in Fig. 1 show that the magnetic field can not be rescaled by $k_B T_H$ or any energy scale proportional to it so as to produce a universal curve for the field-dependent impurity magnetization $\mathcal{M}$. This conclusion applies although the field dependence of $M_{\rm imp}$ is given by a universal function and $\mathcal{M}(B) \propto M_{\rm imp}(B)$ for fixed coupling strength ρJ since the proportionality factor in Eq. (15) depends on the value of ρJ.

To elucidate our findings, we refer to one of the original Bethe ansatz investigations of the Kondo model.[49] With the assumptions of a BA calculation (including an arbitrarily large energy cutoff $\mathscr{D}$), it is found that $\mathcal{M} = M_{\rm imp}$. To study the influence of the cutoff scheme, a comparison with perturbation theory is carried out showing that $\mathcal{M}$ has leading corrections of order $1/\ln(\mathscr{D})$, whereas the corrections of $M_{\rm imp}$ vanish like $1/\mathscr{D}$ and thus much faster.[49] The regime in which all relevant energy scales are negligibly small compared to the cutoff *in a logarithmic sense*, e.g., $\ln(\mathscr{D}/g_S\mu_B B) \gg 1$, is termed "extreme scaling limit."[49] We find these conclusions to be compatible with our NRG results for $\mathcal{M}(B)$ and $M_{\rm imp}(B)$, which demonstrate the following: (1) For $\rho J = J/2W \ll 1$, there is nice agreement with the universal BA solution for $M_{\rm imp}(x, T = 0)$ as long as the Zeeman energy is small compared to W. (2) According to Eq. (15), $\mathcal{M} > M_{\rm imp}$ for $\rho J > 0$. (3) $\mathcal{M}$ approaches $M_{\rm imp}$ if the coupling strength ρJ is reduced. These observations might also bear some importance for experimental situations: While experimental parameters are certainly suitable to consider the scaling regime (in case the system exhibits universal behavior), it is less clear whether an experimental system can be placed in the extreme scaling regime. The difference between $M_{\rm imp}$ and $\mathcal{M}$ is further investigated in Appendix B by studying the coupling-strength dependence of both quantities.

V. IMPURITIES WITH EASY-AXIS ANISOTROPY

We now deal with the case of an impurity with additional easy-axis anisotropy [i.e., with anisotropy parameter $D < 0$ in Eq. (6)]. In this section, emphasis is placed on the field dependence of the impurity magnetization $\mathcal{M}$, again for the case of equal g factors.

Let us begin by briefly recapitulating the magnetic properties of a free spin with easy-axis anisotropy that is described by Hamiltonian (6). For negative anisotropy parameter D and vanishing magnetic field, the ground state of a spin $S \geqslant 1$ is a doublet composed of the states with magnetic quantum number $M = \pm S$. In the special case $S = \frac{1}{2}$, the anisotropy term $D(\underset{\sim}{S}^z)^2$ evaluates to a constant and is thus insignificant for the thermodynamics. The first excited state is a singlet with $M = 0$ for $S = 1$ and a doublet with $M = \pm(S-1)$ for all larger spins. It follows that the energy gap between ground state and first excited state is given by $|D|(2S-1)$. For thermal energies that are small compared to this gap, the zero-field magnetic susceptibility approximately obeys a Curie law with Curie constant $\langle(\underset{\sim}{S}^z)^2\rangle = S^2$ [instead of $S(S+1)/3$ for an isotropic spin].

What do we expect for the full impurity model given by Eq. (1) if there is an additional easy-axis anisotropy? Since the ground-state doublet of the free spin with easy-axis anisotropy has $|\Delta M| = 2S > 1$, the two states it is comprised of are not connected by a single spin flip, which changes M by 1. Furthermore, for increasing values of $|D|$, the gap in the energy spectrum of the free spin with easy-axis anisotropy progressively suppresses scattering processes connecting ground state and first excited state. With this scattering picture in mind, one would thus assume that the complete formation of the Kondo effect is prevented on energy scales smaller than $|D|$. With respect to the impurity magnetization $\mathcal{M}$, there appears to be an even simpler argument: A larger absolute value of the anisotropy parameter D energetically lifts all excited states of the impurity, which have reduced magnetic moment in comparison to the ground-state doublet. At large $|D|$, one would thus expect that the excited states have less weight in the many-body ground state of the full impurity model leading to an increased value of $\mathcal{M}$ at zero temperature for positive magnetic field.

A. Field dependence of the impurity magnetization

In Fig. 2, low-temperature NRG results for the impurity magnetization $\mathcal{M}(B)$ for impurity spin $S = 1, \frac{3}{2}, 2$ are presented. We start the discussion of the results at high magnetic fields and move from there to lower fields. If the Zeeman energy is much larger than the anisotropy parameter, i.e., if $g_S\mu_B B \gg |D|$, nearly isotropic behavior of $\mathcal{M}(B)$ is observed. At smaller fields $g_S\mu_B B \approx |D|$, the impurity magnetization for $D < 0$ begins to deviate from the curve for $D = 0$ and, for $g_S\mu_B B \ll |D|$, converges to a D-dependent value larger than $g_S\mu_B(S - \frac{1}{2})$. In the limit of low fields, the impurity magnetization curves for $D < 0$ shown in Fig. 2 are well described by a linear field dependence:

$$\mathcal{M}(B, T \approx 0) \approx \mathcal{M}_0(D) + \gamma(D) g_S\mu_B B/W. \qquad (16)$$

$\mathcal{M}_0(D)$ thus corresponds to the impurity magnetization in the ground state of Hamiltonian (1) for infinitesimal magnetic field. The low-field behavior for $D < 0$ as described by Eq. (16) is different from that displayed by an isotropic impurity: For $D = 0$ and $S \geqslant 1$, the impurity contribution to the magnetization $M_{\rm imp}(B)$, which is proportional to $\mathcal{M}(B)$ according to Eq. (15), approaches the limit of zero magnetic field with slowly decaying logarithmic corrections.[46,47,72] From the results presented in Fig. 2 we conclude that for nonzero field and $D < 0$ a larger value of $|D|$ leads to a larger impurity magnetization $\mathcal{M}$, with the upper bound for $|D| \to \infty$ given by the free saturation value $g_S\mu_B S$. One might therefore say that an easy-axis anisotropy stabilizes the impurity spin.

Taking another look at Fig. 2 and focusing on the regime of small magnetic fields with $g_S\mu_B B \ll |D|$, one could be misled to think that there is a saturation of the impurity magnetization $\mathcal{M}$ (this impression would not occur for an impurity with $D = 0$). This raises the question as to whether it is possible to approximately describe the field dependence of $\mathcal{M}$ for $g_S\mu_B B \ll |D|$ and nonzero temperature $k_B T \ll |D|$ using a

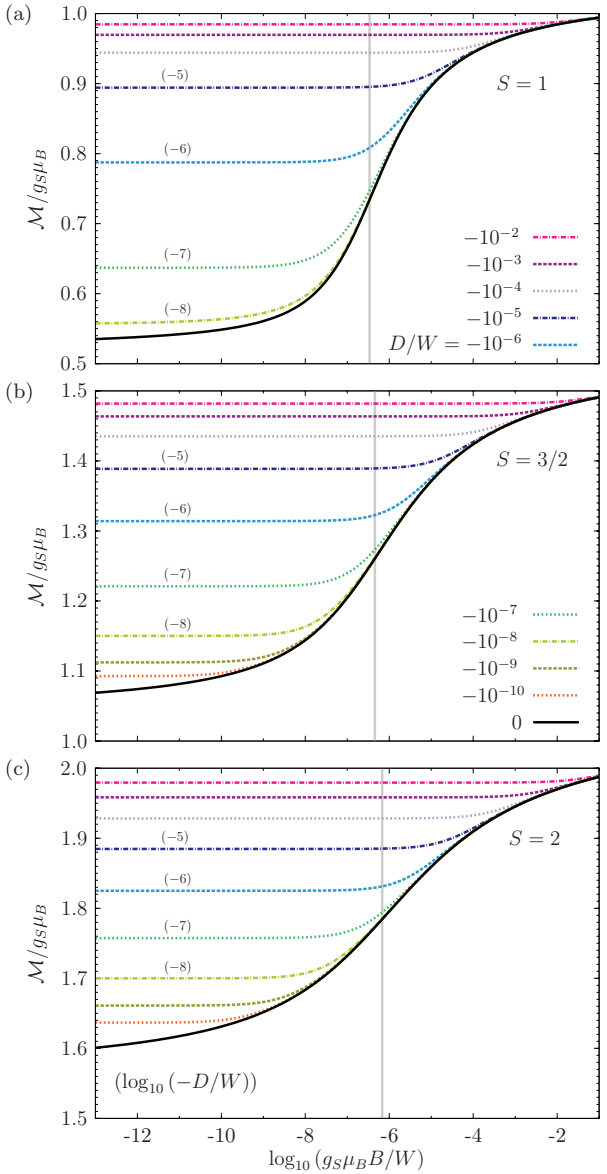

FIG. 2. (Color online) Impurity magnetization $\mathcal{M}$ for different anisotropy parameters $D < 0$ (easy-axis anisotropy) as a function of magnetic field for $k_BT/W \approx 1.54 \times 10^{-15} \approx 0$, coupling strength $\rho J = 0.07$, and impurity spin (a) $S = 1$, (b) $S = \frac{3}{2}$, and (c) $S = 2$. We compare with the magnetization of an impurity with $D = 0$ (solid line). As before, equal g factors of electrons and impurity are assumed. Vertical lines mark the respective value of k_BT_H/W, which is determined by fitting the universal Bethe ansatz solution for $M_{\text{imp}}(T = 0)$ in case of $D = 0$. For $\rho J = 0.07$ and $S = 2$, we find $k_BT_H/W \approx 6.8 \times 10^{-7}$.

model for a free spin. In the simplest case, such a description could be provided by a Brillouin function $B_S(x)$, which gives the temperature and field dependencies of the magnetization of a free and isotropic spin S. As demonstrated in Fig. 3 for one value of D, it is in fact possible to adequately fit the magnetization $\mathcal{M}(B,T > 0)$ for an impurity with easy-axis anisotropy using a rescaled and shifted Brillouin function $\widetilde{B}_S(x) = \gamma B_S(\eta x)$ with free parameters γ and η, as long as $k_BT \ll |D|$ and $g_S\mu_B B \ll |D|$. However, larger fields than those considered in Fig. 3 would reveal that $\mathcal{M}$ is actually not

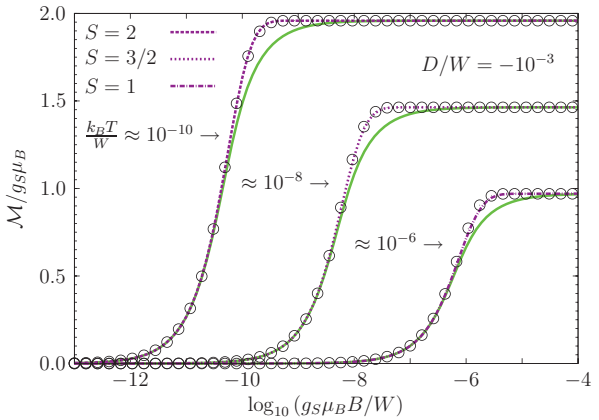

FIG. 3. (Color online) Impurity magnetization $\mathcal{M}$ as a function of magnetic field for anisotropy $D/W = -10^{-3}$ and *nonzero* temperature $k_BT/W \approx 1.03 \times 10^{-6}$ for $S = 1$, $k_BT/W \approx 1.28 \times 10^{-8}$ for $S = \frac{3}{2}$, and $k_BT/W \approx 1.58 \times 10^{-10}$ for $S = 2$. Note that $\mathcal{M}$ is *not* saturated for any field in the plot range (cf. Fig. 2). Open symbols represent fits using a rescaled and shifted Brillouin function $\widetilde{B}_S(x) = \gamma B_S(\eta x)$, and solid (green) lines fits using a rescaled and shifted Langevin function $\widetilde{L}(x) = \gamma L(\eta x)$.

yet saturated (cf. Fig. 2). The ratio of $|D|$ and k_BT_H determines the "apparent saturation value" of $\mathcal{M}$ and thus the parameter γ. In contrast to a fit with a modified Brillouin function, a classical description using a rescaled and shifted Langevin function $\widetilde{L}(x) = \gamma L(\eta x)$ with $L(x) = \lim_{S\to\infty} B_S(x)$ does not work well for magnetic fields close to the "saturation field" (cf. the solid lines in Fig. 3), as expected for a quantum mechanical system with low spin. Nevertheless, a fit using $\widetilde{L}(x)$ can produce reasonable results for fields that are small compared to the "saturation field".

The results depicted in Fig. 3 might be of importance for an experimental study of a system that is (approximately) described by Hamiltonian (1) with a strong easy-axis anisotropy. It is then conceivable that a measurement of the magnetization for magnetic fields that can be realistically produced in an experiment (depending on the value of D, fields with $g_S\mu_B B \approx |D|$ might not be obtainable) does not allow us to distinguish between the magnetic response of an impurity spin with easy-axis anisotropy and that of a free spin. Such a scenario seems more likely if the experimental control over the g factor and the absolute magnitude of the magnetization is limited, and if $|D|$ is large compared to k_BT_H so that the "apparent saturation value" of the impurity magnetization lies close to the free saturation value $g_S\mu_B S$.

B. Impurity contribution to the magnetization and the susceptibility

We have furthermore investigated the relationship between M_{imp} for nonzero magnetic field and the impurity contribution to the susceptibility χ_{imp} at zero field. At low temperature $k_BT \ll |D|$, χ_{imp} obeys a Curie law with a Curie constant that is indicative of a so-called "fractional spin" and interpolates between the free isotropic value of $S(S+1)/3$ for $|D| \to 0$ and the free anisotropic low-temperature value of S^2 for $|D| \to \infty$.[63] It turns out that there is a simple relation between the Curie constant and the low-temperature magnetization M_{imp}

for small magnetic fields $g_S\mu_B B \ll |D|$:

$$\left.\frac{k_B T\,\chi_{\rm imp}}{(g_S\mu_B)^2}\right|_{B=0,\ k_BT\ll|D|} \approx \left.\left(\frac{M_{\rm imp}}{g_S\mu_B}\right)^2\right|_{\tilde h\ll|D|,\ k_BT\ll\tilde h}, \qquad (17)$$

with $\tilde h = g_S\mu_B B$. The relative deviation between the left- and right-hand sides of Eq. (17), as determined by NRG calculations for all parameter combinations used in Fig. 2, is less than 1‰. The relationship between zero-field susceptibility and magnetization expressed by Eq. (17) shows that the magnetic response of the fractional spin at low temperature and field corresponds to that of an ordinary doublet composed of states with magnetic quantum numbers $\pm M$ (in particular, a free spin with easy-axis anisotropy effectively reduces to such a doublet at low temperature $k_BT \ll |D|$, as discussed at the beginning of this section). This conclusion is in line with the temperature dependence of the impurity contribution to the entropy at zero field, which approaches the value $S_{\rm imp} = k_B \ln 2$ for $k_BT \ll |D|$.[63]

VI. IMPURITIES WITH HARD-AXIS ANISOTROPY

We now investigate how an additional hard-axis anisotropy ($D > 0$) affects the magnetic properties of the impurity spin. To lay the foundations for a study of the full impurity problem, we first discuss the magnetic field dependence of the magnetization for a free spin with hard-axis anisotropy that is described by Hamiltonian (6) with $D > 0$.

For positive D and $B = 0$, the eigenvalues of Hamiltonian (6) are energetically ordered according to the absolute value of their magnetic quantum number M. Depending on the spin S, the ground state is thus either a singlet with $M = 0$ (for integer S) or a doublet with $M = \pm\frac{1}{2}$ (for half-integer S). In either case, the rest of the energy spectrum consists of doublets with magnetic quantum numbers $\pm M$ and $\frac{1}{2} < M \leqslant S$. The energy gap $\Delta_{|M|}$ between a level with quantum number M and the next higher-lying doublet is given by $\Delta_{|M|} = (2|M| + 1)D$. As a consequence of the magnetic field dependence of the energy levels due to the Zeeman term in Eq. (6), n ground-state level crossings occur for positive magnetic fields, with $n = S$ for integer spin and $n = S - \frac{1}{2}$ for half-integer spin. At the field $B_M = \Delta_{|M|}/g_S\mu_B$, the magnetic quantum number of the ground state abruptly changes from $-M$ to $-(M + 1)$ and hence the zero-temperature magnetization curve displays a discontinuous step. This connection is illustrated in Fig. 4 for spin $S = 1$, $\frac{3}{2}$, and 2. Nonzero temperature smears out the magnetization steps and renders them continuous. As the low-energy situation is the same in the vicinity of each ground-state level crossing, so is the effect of moderate temperature [cf. Fig. 4(c)].

Since the ground state of a free spin with hard-axis anisotropy *in zero magnetic field* differs for integer and half-integer spins, the properties of the full impurity model (1) with $D > 0$ and $B = 0$ also depend on the impurity spin S.[63] A simplified picture applies for large ratios $D/k_BT_H \gg 1$. In this case, little Kondo screening can occur for decreasing temperature before the anisotropy becomes effective on the energy scale $k_BT \approx D$ and higher-lying impurity states are frozen out.[63] The impurity spin is then approximately reduced to the ground state of the corresponding free spin with $D > 0$.[63] For integer S, this is a nonmagnetic singlet. In contrast, a doublet with $M \approxeq \pm\frac{1}{2}$ is effectively formed for half-integer impurity spin. In Ref. 63, it is shown that this doublet undergoes pseudo-spin-$\frac{1}{2}$ Kondo screening at low temperature $k_BT \ll D$. The observed Kondo effect is described by an anisotropic exchange interaction which reflects that the effective doublet emerges from the original impurity spin multiplet.[63]

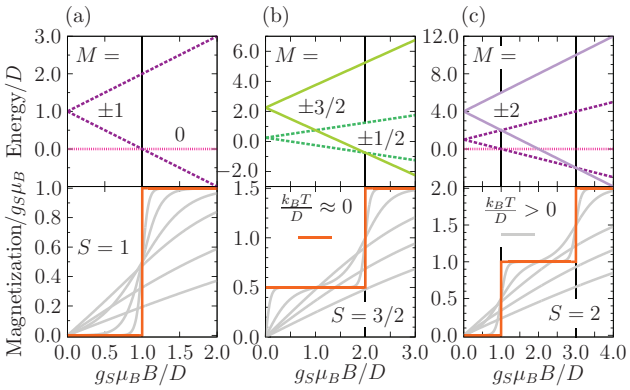

FIG. 4. (Color online) Energy levels with magnetic quantum numbers M (upper panels) and magnetization (lower panels) as a function of magnetic field for an anisotropic spin, described by Hamiltonian (6) with $D > 0$ (hard-axis anisotropy), with (a) $S = 1$, (b) $S = \frac{3}{2}$, and (c) $S = 2$. For the magnetization curves and fields larger than the respective saturation field, temperature increases from top to bottom.

For a free spin with hard-axis anisotropy in nonzero magnetic field, Fig. 4 demonstrates that the two energy levels which form the degenerate ground state at a level crossing field have magnetic quantum numbers differing by $|\Delta M| = 1$. This means that the two levels are connected by a single spin flip. For the full impurity model (1) with $D/k_BT_H \gg 1$, we therefore expect that at certain magnetic fields and for low temperature $k_BT \lesssim D$ the impurity spin is effectively reduced to a doublet with $|\Delta M| \approxeq 1$ so that a "field-induced" pseudo-spin-$\frac{1}{2}$ Kondo effect can arise. In particular, the screening should be exchange anisotropic as the impurity spin is again restricted to a subset of all its states for $k_BT \lesssim D$. Since all free spins with hard-axis anisotropy display ground-state level crossings, these field-induced Kondo effects ought to be observable for arbitrary impurity spin $S \geqslant 1$ at $D/k_BT_H \gg 1$. Furthermore, for large D the number of field-induced Kondo effects is expected to match the number of ground-state level crossings that occur for the corresponding free spin with $D > 0$.

A. Magnetic field dependence of the impurity magnetization

We begin with a discussion of the magnetic field dependence of the impurity magnetization $\mathcal{M}(B)$ for equal g factors and quasivanishing temperature $T \approx 0$. Magnetization curves for impurity spin $S = 1$, $\frac{3}{2}$, and 2 and several values of the anisotropy parameter $D > 0$ are shown in Fig. 5. Since the coupling strength ρJ, and thus the energy scale k_BT_H according to Table I, is kept constant, the ratio D/k_BT_H is varied. It turns out that this ratio determines the qualitative behavior of the impurity magnetization curves. Note that a linear magnetic field scale is used in Fig. 5 to allow for an

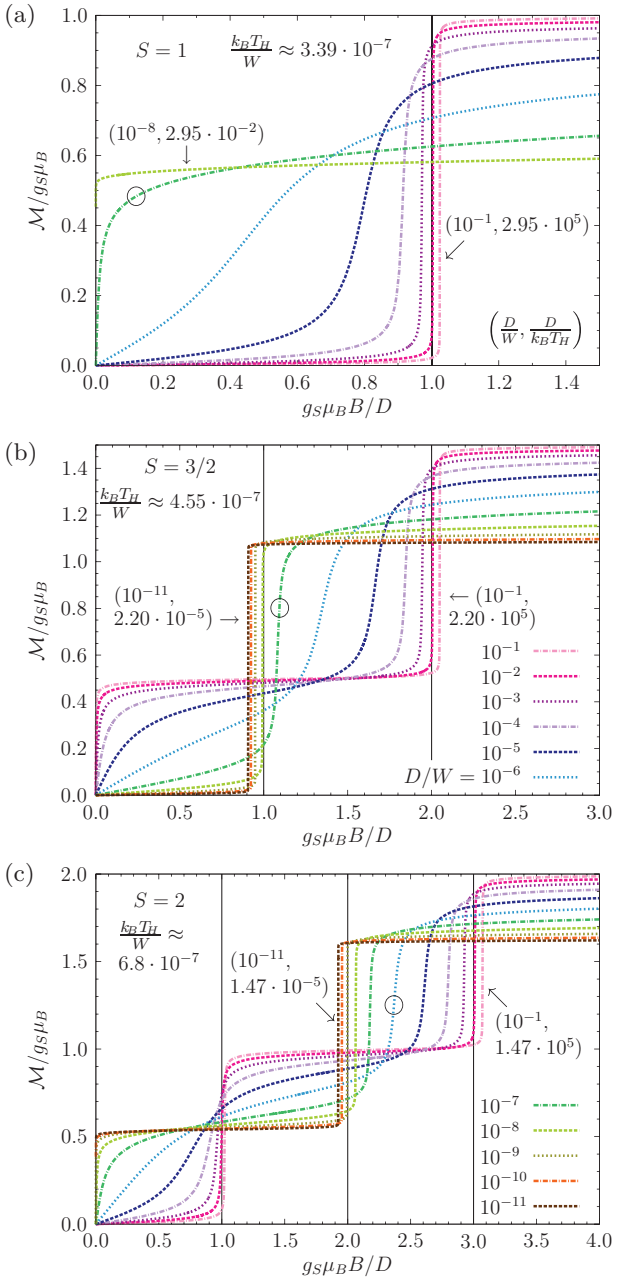

FIG. 5. (Color online) Impurity magnetization $\mathcal{M}$ for varying hard-axis anisotropy $D > 0$ as a function of magnetic field for temperature $k_B T/W \approx 1.54 \times 10^{-15} \approx 0$, coupling strength $\rho J = 0.07$, equal g factors, and impurity spin (a) $S = 1$, (b) $S = \frac{3}{2}$, and (c) $S = 2$. The value of D increases from bottom to top or from left to right, respectively. Note the rescaling of the Zeeman energy $g_S\mu_B B$ by D. Circles indicate those magnetization curves for which $|(D - k_B T_H)/W|$ is minimal.

easy comparison with the results for a free spin with hard-axis anisotropy from Fig. 4.

For an interpretation of the results for $\mathcal{M}(B, T \approx 0)$, let us first consider the two limiting cases in which D is either small or large compared to $k_B T_H$. In the following, imagine that we move from large magnetic fields to lower fields. If D is large, then little Kondo screening can occur before the anisotropy becomes effective. As a *guideline*, we might thus think of the energy spectrum of a free spin S with hard-axis anisotropy. On the other hand, for small D significant Kondo screening can take place before the magnetic field reaches the energy scale defined by the anisotropy, so that it eventually becomes more appropriate to think of the energy levels of a free spin $S - \frac{1}{2}$ with hard-axis anisotropy. As illustrated in Fig. 4, ground-state level crossings occur for a spin with hard-axis anisotropy at certain fields and give rise to steps in the zero-temperature magnetization curve. For small and large anisotropy D, the impurity magnetization $\mathcal{M}(B, T \approx 0)$ also displays sharp, steplike features that are surrounded by magnetic field domains in which $\mathcal{M}$ only slowly increases with B ("pseudoplateaux"). However, due to the energy continuum of electronic states, these sharp features remain continuous even in the limit of zero temperature. The number of steps and their position relative to the field $D/g_S\mu_B$ depend on the impurity spin S for large D and on the residual spin $S - \frac{1}{2}$ for small D, respectively. The case $S = 1$ is special because the residual spin-$\frac{1}{2}$ can not have uniaxial anisotropy. The single step which exists for $S = 1$ at large D therefore disappears for smaller values of D. With respect to the energy scale imposed by the anisotropy, the steps in the impurity magnetization curves become well defined for small and large D [cf. Figs. 5(b) and 5(c)]. In addition, the pseudoplateaux become flatter. Figure 5(c) furthermore suggests that the two steps appearing in $\mathcal{M}(B, T \approx 0)$ for $S = 2$ and large D have different width. We are going to discuss the aspect of step width in more detail in Sec. VI B. In particular, it will be shown that an impurity magnetization step is steeper if it occurs at larger field. It turns out that a standard z averaging of the NRG results introduces artifacts into the magnetization steps for large anisotropy D. This problem is investigated in more detail in the context of an effective model in Appendix D. The plots shown in Fig. 5 are not visibly affected by this numerical shortcoming.

The position of the steps in the impurity magnetization curves for both small and large anisotropy D compared to $k_B T_H$ seems interesting. Figures 5(b) and 5(c) show that for small D and impurity spin $S = \frac{3}{2}$ and $S = 2$, a step occurs at a magnetic field which is smaller than the corresponding level crossing field for a free spin $S - \frac{1}{2}$ with hard-axis anisotropy (cf. Fig. 4). In contrast, for large D and all three impurity spins considered in Fig. 5, each impurity magnetization step is found at a field exceeding the corresponding level crossing field for a free spin S with $D > 0$. One might wonder whether the half-bandwidth W of the electrons has an impact on these two effects. To investigate this question for the case of small anisotropy, we have calculated additional magnetization curves for impurity spin $S = \frac{3}{2}$ and 2 with decreasing coupling strength ρJ (0.09, 0.07, and 0.05). Since $\rho = 1/2W$, a reduction of ρJ can be interpreted as an increase of the half-bandwidth W for constant J. For each value of the coupling strength, the anisotropy parameter was chosen so as to give a constant ratio $D/k_B T_H = 10^{-3}$ according to Table I. With this choice of D, a reduction of ρJ leads to a shift of the step in the impurity magnetization curve towards smaller fields *relative to* $D/g_S\mu_B$. This suggests that the effect observed for small D is not bandwidth related. The question at which fields impurity magnetization steps occur for large anisotropy is investigated in Sec. VI B.

The limiting cases of small and large anisotropy D compared to k_BT_H are connected by a regime with partial Kondo screening in which it is not possible to exclusively think in terms of the impurity spin S or a residual spin $S-\frac{1}{2}$. Impurity magnetization steps are broadened in this regime with respect to the energy scale D and, upon reducing the anisotropy parameter, move towards lower fields relative to $D/g_S\mu_B$ [see Fig. 5(b)]. In addition, one step disappears for $D \approx k_BT_H$ in case of integer impurity spin [cf. Fig. 5(c)]. Kondo screening effectively changes the impurity spin S from integer to half-integer and vice versa. Depending on the ratio D/k_BT_H and the resulting degree of Kondo screening, different behavior of the impurity magnetization is therefore observed, in particular for fields $g_S\mu_BB \lesssim D$: While there is little magnetic response for an effective integer spin (at zero temperature, there is none at all for a free integer spin with hard-axis anisotropy as shown in Fig. 4), we have larger impurity magnetization $\mathcal{M} \approx g_S\mu_B/2$ for effective half-integer spin. However, in the latter case, an additional pseudo-spin-$\frac{1}{2}$ Kondo effect occurs[63] which leads to a suppression of the impurity magnetization for magnetic fields $g_S\mu_BB \ll D$.

In order to study the three different anisotropy regimes ($D/k_BT_H \ll 1$, $D/k_BT_H \approx 1$, and $D/k_BT_H \gg 1$) in more detail, selected impurity magnetization curves from Fig. 5 are replotted using a logarithmic magnetic field scale (see Figs. 6–8). This brings out pseudo-spin-$\frac{1}{2}$ Kondo effects more clearly and allows for a better comparison with the magnetization of an impurity with $D=0$. Figures 6–8 furthermore demonstrate the effect of nonzero temperature on the impurity magnetization in case of hard-axis anisotropy.

At large magnetic field $g_S\mu_BB \gg D$, the magnetization curve $\mathcal{M}(B,T\approx 0)$ for an impurity with hard-axis anisotropy closely resembles the result for $D=0$. For lower fields $g_S\mu_BB \gtrsim D$, the anisotropy eventually becomes effective and the impurity magnetization begins to deviate from the curve for $D=0$. In this sense, an additional hard-axis anisotropy prevents the Kondo screening, which would reduce the impurity spin S to an residual spin $S-\frac{1}{2}$ in the limit $g_S\mu_BB/k_BT_H \to 0$ for $D=0$, from completing. The ratio D/k_BT_H controls the extent of Kondo screening on the energy scale D. In particular, it determines whether the number and approximate position of the steps in the zero-temperature impurity magnetization curve correspond to the magnetic response of a free spin S with $D>0$ (for $D/k_BT_H \gg 1$ and little Kondo screening, cf. Fig. 4) or a free spin $S-\frac{1}{2}$ with $D>0$ (for $D/k_BT_H \ll 1$ and considerable Kondo screening).

$\mathcal{M}(B,T\approx 0)$ displays a linear dependence on B for Zeeman energies that are small compared to all relevant energy scales. If temperature is high so that $k_BT \gg D$, then $\mathcal{M}(T,B)$ is suppressed for magnetic fields of the order of and smaller than $k_BT/g_S\mu_B$. On the other hand, judging by the relative deviation from the zero-temperature curve, finite temperature has a negligible effect on the impurity magnetization if the thermal energy falls into the energy regime in which $\mathcal{M}(B,T\approx 0) \propto B$ (such a temperature independence is known for an impurity with $S=\frac{1}{2}$, as discussed in Sec. IV A). In this regard, $\mathcal{M}$ differs from the magnetization of a free spin with hard-axis anisotropy for which nonzero temperature is always relevant. If the impurity magnetization curve features steps, they are smeared out for sufficiently high temperature. In case there is more than one step in $\mathcal{M}(B,T\approx 0)$ [cf. Fig. 8(a)], then, as a further difference compared to a free

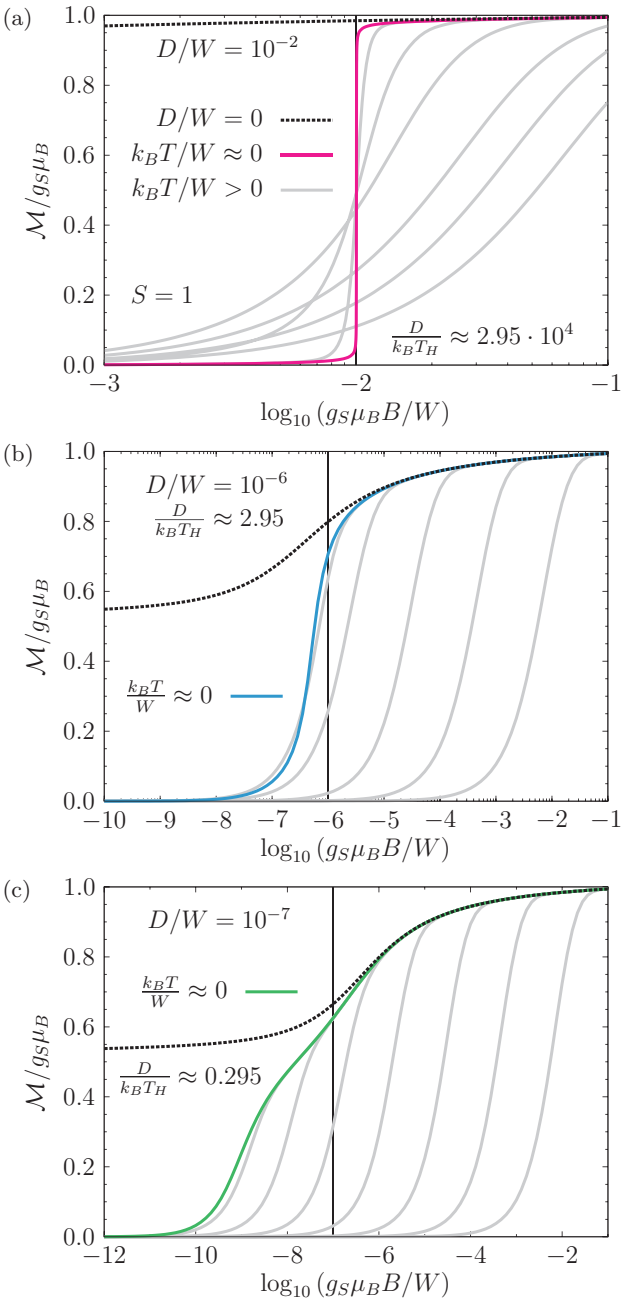

FIG. 6. (Color online) Impurity magnetization $\mathcal{M}$ as a function of magnetic field for impurity spin $S=1$ and anisotropy parameter (a) $D/W = 10^{-2}$, (b) $D/W = 10^{-6}$, and (c) $D/W = 10^{-7}$ (solid lines, cf. Fig. 5). Dashed lines show $\mathcal{M}(B)$ for $D=0$ and $k_BT/W \approx 1.54 \times 10^{-15} \approx 0$. For the light gray lines, the approximate value of k_BT/W increases from left to right from (a) 4.35×10^{-4} to 6.10×10^{-2}, (b) 1.99×10^{-7} to 6.79×10^{-3}, and (c) 4.73×10^{-10} to 6.79×10^{-3}. Adjacent finite-temperature curves in plots (b) and (c) are calculated using truncated Wilson chains whose lengths differ by either four or five lattice sites. Thin vertical lines indicate the respective Zeeman energy $g_S\mu_BB = D$. For the chosen coupling strength $\rho J = 0.07$ and $D=0$, we have $k_BT_H/W \approx 3.39 \times 10^{-7}$ according to Table I.

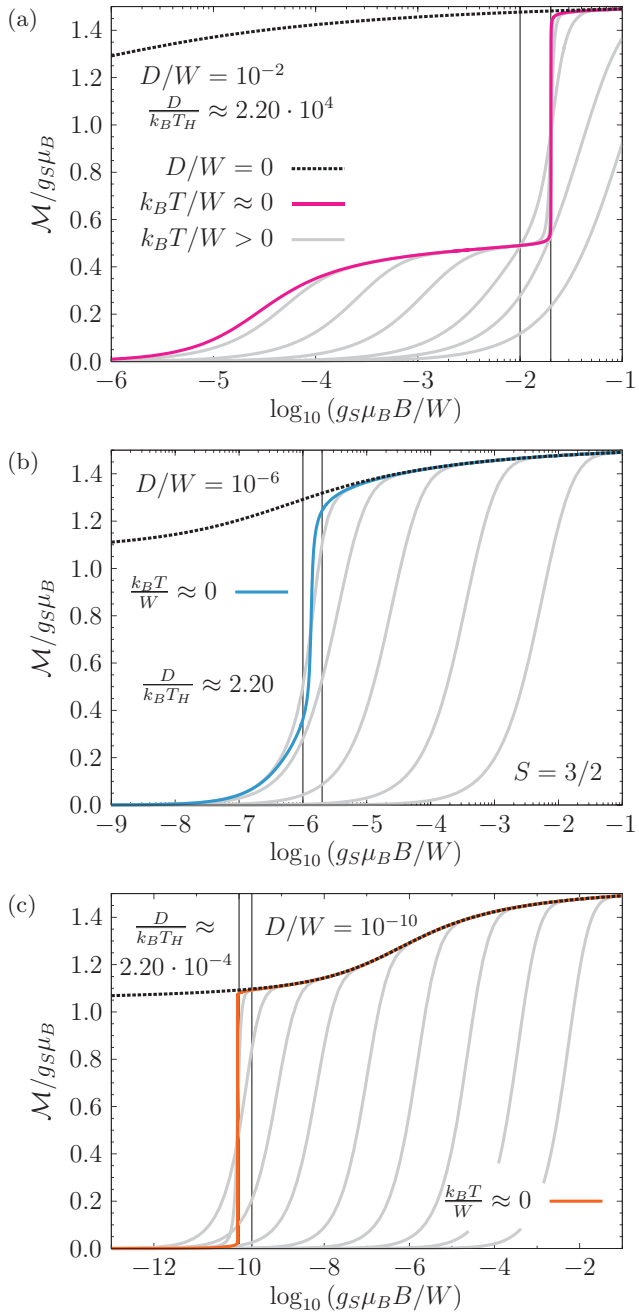

FIG. 7. (Color online) Impurity magnetization $\mathcal{M}$ as a function of magnetic field for impurity spin $S = \frac{3}{2}$ and anisotropy parameter (a) $D/W = 10^{-2}$, (b) $D/W = 10^{-6}$, and (c) $D/W = 10^{-10}$ (solid lines, cf. Fig. 5). As before, dashed lines show $\mathcal{M}(B)$ for $D = 0$ and $k_B T/W \approx 0$. For the light gray lines, the approximate value of $k_B T/W$ increases from left to right from (a) 1.61×10^{-5} to 1.05×10^{-1}, (b) 3.45×10^{-7} to 6.79×10^{-3}, and (c) 1.01×10^{-11} to 6.79×10^{-3}. Adjacent finite-temperature curves in plots (b) and (c) are again calculated using truncated Wilson chains whose lengths differ by either four or five lattice sites. Magnetic fields satisfying $g_S\mu_B B = nD$ with $n = 1,2$ are highlighted by thin vertical lines. According to Table I, $k_B T_H/W \approx 4.55 \times 10^{-7}$ for $\rho J = 0.07$ and $D = 0$.

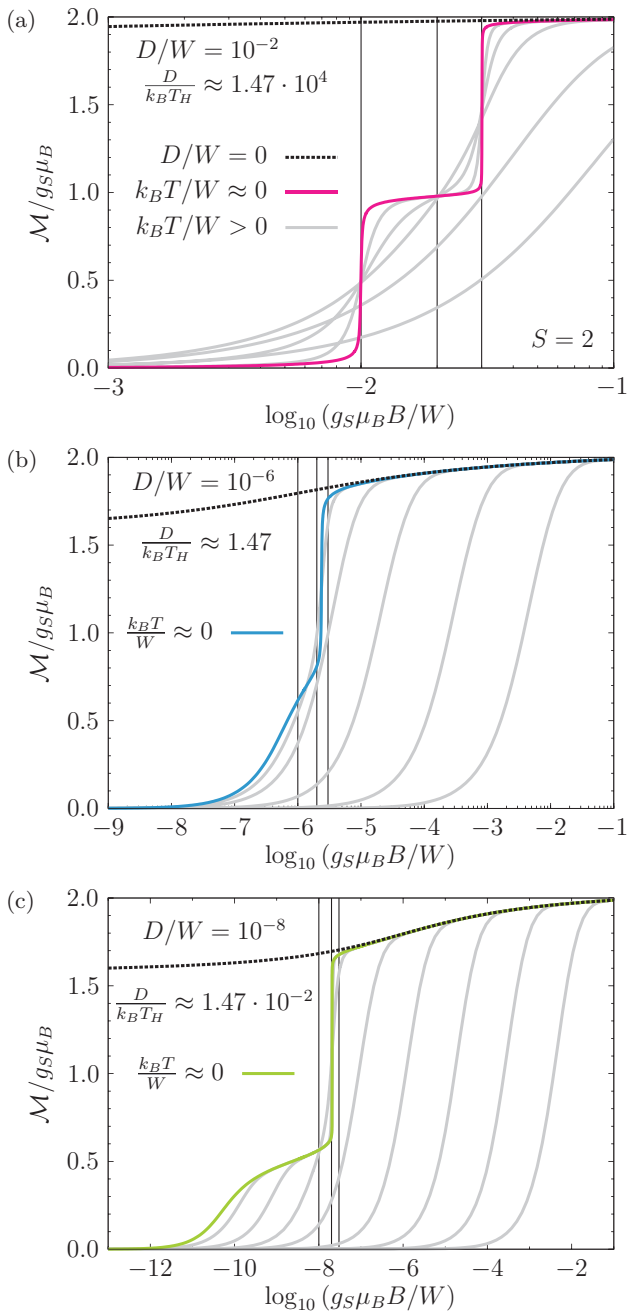

FIG. 8. (Color online) Impurity magnetization $\mathcal{M}$ as a function of magnetic field for impurity spin $S = 2$ and anisotropy parameter (a) $D/W = 10^{-2}$, (b) $D/W = 10^{-6}$, and (c) $D/W = 10^{-8}$ (solid lines, cf. Fig. 5). Dashed lines again show $\mathcal{M}(B)$ for $D = 0$ and $k_B T/W \approx 0$. For the light gray lines, the approximate value of $k_B T/W$ increases from left to right from (a) 7.54×10^{-4} to 1.05×10^{-1}, (b) 3.45×10^{-7} to 6.79×10^{-3}, and (c) 5.26×10^{-11} to 6.79×10^{-3}. Adjacent finite-temperature curves in plots (b) and (c) are calculated using truncated Wilson chains whose lengths differ by four to six lattice sites. Thin vertical lines indicate magnetic fields satisfying $g_S\mu_B B = nD$, with $n = 1,2,3$. For $\rho J = 0.07$ and $D = 0$, we obtain $k_B T_H/W \approx 6.8 \times 10^{-7}$.

spin with hard-axis anisotropy, nonzero temperature has an unequal effect on the different steps. We come back to the last two observations in Sec. VI B.

The results in the regime of small magnetic fields $g_S\mu_B B \ll D$ can be related to the zero-field study of Ref. 63. According to the physical picture of the case $B = 0$ summarized at

the beginning of Sec. VI, the low-temperature impurity magnetization is either suppressed if the impurity spin is effectively reduced to a singlet [see Figs. 6(a), 7(c), and 8(a)], or it reflects the magnetic response of a Kondo screened pseudo-spin-$\frac{1}{2}$ doublet [cf. Figs. 6(c), 7(a), and 8(c)]. For small D and integer impurity spin, the corresponding Kondo temperature decreases faster than linear in D upon reducing the anisotropy (it even drops exponentially fast in the special case $S = 1$).[63] As a result, the pseudoplateau that appears for $S = 2$ at magnetic fields $g_S\mu_B B \lesssim 2D$ [see Figs. 5(c) and 8(c)] becomes flatter and broader when decreasing D, whereas a reduction of D eventually leads to quasi-isotropic behavior over the whole considered magnetic field range for $S = 1$ [see Figs. 5(a) and 6(c)]. On the other hand, for large and increasing anisotropy D and half-integer impurity spin, the observed screening effect is increasingly well described by an exchange-anisotropic $S = \frac{1}{2}$ Kondo model, whose Kondo temperature has a value much smaller than W/k_B.[63] This means that the pseudoplateau occurring for impurity spin $S = \frac{3}{2}$ and fields $g_S\mu_B B \lesssim 2D$ [see Figs. 5(b) and 7(a)] becomes more pronounced for larger anisotropy D. As a final remark, Fig. 8(a) once again shows the different width of the two impurity magnetization steps for $S = 2$ and large D.

In Appendix C, we investigate how the magnetization curves $\mathcal{M}(B,T \approx 0)$ are affected by the ratio g_e/g_S of electron and impurity g factor. It turns out that the difference between the impurity magnetization for a local and a bulk magnetic field can be related to the connection between $\mathcal{M}$ and M_{imp} for equal g factors. In case of the single-impurity Anderson model, the impurity contribution to the zero-field susceptibility for $g_e = 0$ and g_S has been recently studied in Ref. 78. In accordance with the Clogston-Anderson compensation theorem (see Ref. 72), it is found that the two susceptibilities are nearly identical for all considered temperatures.

B. Field-induced Kondo effects

In order to better understand the steps in the low-temperature magnetization curves for large anisotropy $D > 0$ [cf. Figs. 5 and 9(a)], we now derive effective models near ground-state level crossings (LCs) of the corresponding free spin with hard-axis anisotropy (see Fig. 4). These models are approximations to the full Hamiltonian in the limit of large D.

1. *Effective models near ground-state level crossings in the limit of arbitrarily large anisotropy*

For given impurity spin $S \geqslant 1$ let us consider one of the ground-state level crossings of the corresponding free spin with hard-axis anisotropy (cf. Fig. 4). If D is large, then the two levels which cross in the ground state are energetically well separated from the rest of the spectrum in the vicinity of the LC field. As an approximation for the full impurity model *near this free LC field*, we therefore project the impurity degrees of freedom in Hamiltonian (1) onto the two impurity states involved in the free LC. This way, the impurity Hilbert space is reduced to two states and the impurity spin S can thus be mapped to an effective spin-$\frac{1}{2}$. While the projection becomes exact only in the limit $D \to \infty$, we expect it to be a quantitative approximation for $D \gg W$ and $D \gg k_B T$.

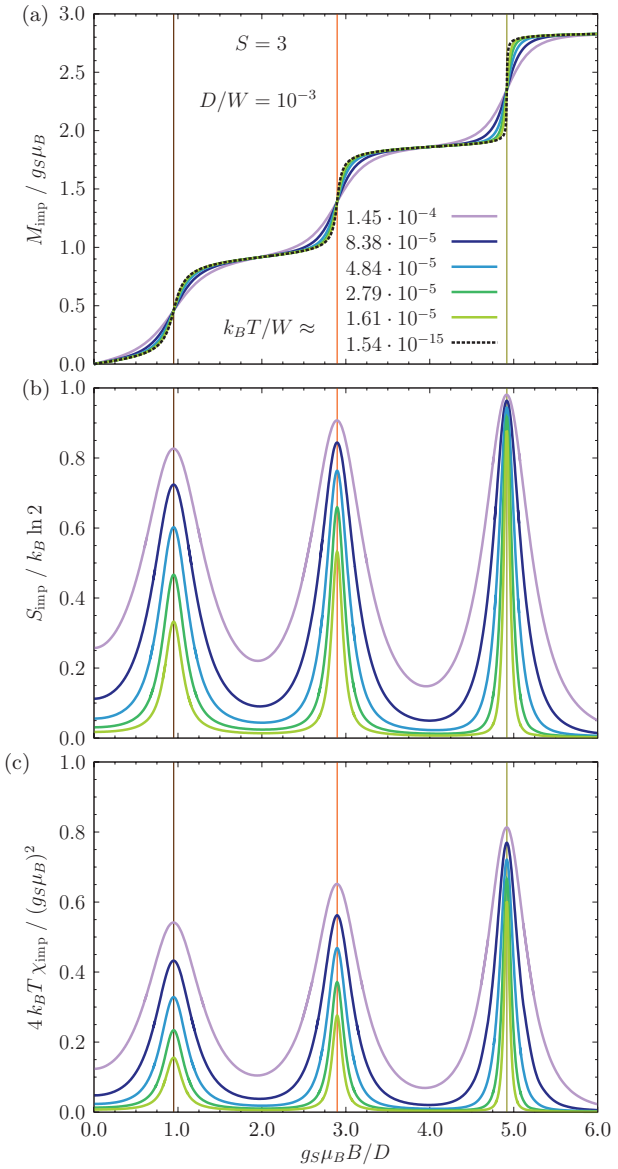

FIG. 9. (Color online) Impurity contribution to (a) the magnetization M_{imp}, (b) the entropy S_{imp}, and (c) the effective moment $T\chi_{\text{imp}}$ as a function of magnetic field for impurity spin $S = 3$, hard-axis anisotropy $D/W = 10^{-3}$, and several temperature values. In plot (a), the dashed curve shows $M_{\text{imp}}(B)$ for $k_BT/W \approx 0$, and for the curves in plots (b) and (c) temperature increases from bottom to top. Thin vertical lines indicate the (equal) peak positions for $S_{\text{imp}}(B)$ and $T\chi_{\text{imp}}(B)$. As before, the coupling strength is chosen as $\rho J = 0.07$ and equal g factors are used.

The mapping of the impurity spin to a pseudo-spin-$\frac{1}{2}$ is an extension of the ideas from Refs. 63 and 68. In contrast to the case of zero magnetic field that has been studied there, we do not project onto impurity doublets with $M = \pm\frac{1}{2}$ (see following). Furthermore, at each LC, i.e., for each step in the magnetization curve, the impurity is reduced to a different pair of states. As a consequence, different parameters of the effective model are obtained at each LC.

We intend to use the effective models to determine the magnetic fields at which steps appear in the impurity magnetization curves for large anisotropy D (cf. Fig. 5), and to investigate

how the properties of the full impurity model differ near the various free LCs [as indicated, e.g., by Fig. 9(a)]. Compared to the full model, the effective models are numerically less demanding as they feature a spin-$\frac{1}{2}$ impurity independent of the value of S, and they allow us to study the effect of the different terms appearing in the effective Hamiltonian.

To be specific, we consider the two impurity states with magnetic quantum numbers $-M$ and $-(M+1)$ (assuming $M \geqslant 0$), which cross at the free LC field $B_M = (2M+1)D/g_S\mu_B$, and project the impurity and interaction part of Hamiltonian (1) onto them. The effective model is determined by requiring that its matrix representation be equal to that of the full model in the chosen subspace. Note that we have to introduce new impurity states by shifting the magnetic quantum number in order to map the impurity spin to a pseudo-spin-$\frac{1}{2}$. This mapping then corresponds to the following replacements for the impurity spin operators:

$$\underset{\sim}{S}^x \;\to\; \sqrt{(S-M)(S+M+1)}\;\underset{\sim}{s}^x, \tag{18}$$

$$\underset{\sim}{S}^y \;\to\; \sqrt{(S-M)(S+M+1)}\;\underset{\sim}{s}^y, \tag{19}$$

$$\underset{\sim}{S}^z \;\to\; \underset{\sim}{s}^z - (M+1/2)\,\underset{\sim}{\mathbb{1}}_s. \tag{20}$$

The impurity formally has spin $s = \frac{1}{2}$ now and the replacement for $(\underset{\sim}{S}^z)^2$ directly follows from that for $\underset{\sim}{S}^z$. In the parameter regime in which the projection is valid, the mapping for $\underset{\sim}{S}^z$ leads to the following connection between the impurity magnetization of the full and effective model:

$$\mathcal{M}/g_S\mu_B = -\langle \underset{\sim}{S}^z\rangle \approx -\langle \underset{\sim}{s}^z\rangle + (M+1/2). \tag{21}$$

There is an analogous relationship for the impurity contribution to the magnetization M_{imp}, as seen from Eq. (11). According to its definition, the impurity contribution to the magnetic susceptibility χ_{imp} is not affected by the shift of the magnetic quantum numbers.

Applying mappings (18) to (20) to the full impurity model (1) and dropping all constant terms, the following Hamiltonian is obtained:

$$\begin{aligned}\underset{\sim}{H}_s(S,M) = &\sum_{\boldsymbol{k},\sigma} \varepsilon_{\boldsymbol{k}\sigma}\, \underset{\sim}{c}^\dagger_{\boldsymbol{k}\sigma}\underset{\sim}{c}_{\boldsymbol{k}\sigma} - \kappa\, \underset{\sim}{s}^z_0 \\ &+ J_\perp\left(\underset{\sim}{s}^x_0\underset{\sim}{s}^x + \underset{\sim}{s}^y_0\underset{\sim}{s}^y\right) + J_\parallel \underset{\sim}{s}^z_0\underset{\sim}{s}^z \\ &+ g_S\mu_B(B-B_M)\underset{\sim}{s}^z,\end{aligned} \tag{22}$$

with the set of parameters

$$\varepsilon_{\boldsymbol{k}\sigma} = \varepsilon_{\boldsymbol{k}} + \sigma g_e\mu_B B \quad (\sigma = \pm 1/2), \tag{23}$$

$$\kappa = (M+1/2)\,J, \tag{24}$$

$$J_\perp = \sqrt{(S-M)(S+M+1)}\,J, \tag{25}$$

$$J_\parallel = J, \tag{26}$$

$$B_M = (2M+1)D/g_S\mu_B. \tag{27}$$

In contrast to the full Hamiltonian, $\underset{\sim}{H}_s(S,M)$ is exchange anisotropic with $J_\perp > J_\parallel$: $J_\perp/J_\parallel$ grows with S and decreases with increasing M (while always present, the exchange anisotropy thus becomes weaker with every further LC). The Zeeman term for the impurity is now expressed relative to the free LC field B_M. $\underset{\sim}{H}_s(S,M)$ furthermore contains the new term $-\kappa\,\underset{\sim}{s}^z_0$ representing an effective magnetic field, which couples to the electron spin at the origin and points in the opposite direction of the external field B. With respect to NRG, this term can be regarded as spin-dependent scattering at the zeroth site of the Wilson chain. It breaks the invariance under a spin-flip transformation [$\underset{\sim}{c}_{\boldsymbol{k}\sigma} \to \underset{\sim}{c}_{\boldsymbol{k}-\sigma}$ and $\underset{\sim}{\boldsymbol{s}} \to (\underset{\sim}{s}^x, -\underset{\sim}{s}^y, -\underset{\sim}{s}^z)$], which $\underset{\sim}{H}_s(S,M)$ would otherwise possess for $B = B_M$. While the scattering parameter κ grows with M, the ratio κ/B_M is independent of M. Starting with the second LC, κ is larger than $J_\parallel$. The ratio $\kappa/J_\perp$, which at first is smaller than 1, also grows with M and eventually becomes greater than 1 if S is large enough.

As an analog to the free LC field B_M, we call the magnetic field B_{ELC} for which the impurity magnetization vanishes at zero temperature (i.e., the two impurity levels are effectively degenerate) "effective level crossing (ELC) field":

$$\langle \underset{\sim}{s}^z\rangle(B_{\mathrm{ELC}}, T=0) = 0. \tag{28}$$

In the parameter regime in which the mapping to a pseudo-spin-$\frac{1}{2}$ is valid, there is a step in the impurity magnetization curve of the full model at the ELC and, according to Eq. (21), the value of $\mathcal{M}$ at the ELC field is $\mathcal{M}(B_{\mathrm{ELC}}, T=0) \approx g_S\mu_B(M+\frac{1}{2})$. In the following, we discuss the properties of Hamiltonian (22) in more detail for the two different cases $g_e > 0$ and $g_e = 0$.

Let us begin with the case $g_e > 0$. As the free LC field B_M is proportional to D, the limit $D \to \infty$ also corresponds to the limit $B \to \infty$. A nonzero Zeeman coupling of the electrons therefore leads to their complete polarization so that formally they may be replaced with spinless fermions (corresponding to spin-down electrons). Since the remaining fermion band is then completely filled, all interaction terms vanish and the electrons can be completely eliminated from the problem. For $g_e > 0$ and arbitrarily large D, Hamiltonian (22) thus reduces to a pure spin model

$$\underset{\sim}{H}^{(g_e>0)}_{\mathrm{eff}}(\widetilde{B}) = g_S\mu_B\left(\widetilde{B} - \frac{J/2}{g_S\mu_B}\right)\underset{\sim}{s}^z. \tag{29}$$

Here, we have introduced a relative magnetic field $\widetilde{B} = B - B_M$. As the only remnant of the interaction between impurity and electrons, a shift of the free LC field remains. This shift is positive for antiferromagnetic coupling $J > 0$ and only depends on the coupling strength, but not on S or M. It is thus the same for all LCs. From the effective model (29) we learn that the ELC fields eventually exceed the free LC fields for $g_e > 0$ and large anisotropy D (cf. Fig. 5).

We now turn to the case of a local magnetic field. Setting $g_e = 0$ and using the relative field $\widetilde{B}$, Hamiltonian (22) becomes the effective model for arbitrarily large D:

$$\underset{\sim}{H}^{(g_e=0)}_{\mathrm{eff}}(\widetilde{B}; S, M) = \underset{\sim}{H}_s(S,M)|_{g_e=0}. \tag{30}$$

We are particularly interested in the properties of $\underset{\sim}{H}^{(g_e=0)}_{\mathrm{eff}}(\widetilde{B}; S, M)$ at the ELC field $\widetilde{B}_{\mathrm{ELC}} = B_{\mathrm{ELC}} - B_M$. Due to the scattering term, the effective model does not exhibit a spin-flip invariance at the ELC. It therefore seems that the ELC is not characterized by special symmetry properties. A spin-*independent* (potential) scattering term can be treated

by transforming to scattering states which diagonalize the electronic part of the Hamiltonian (cf. Appendix C of Ref. 79). Although such a transformation can be easily adapted to the case of spin-*dependent* scattering, it does not seem to yield the intended results. The approximation which is used in the spin-independent case (a modification of the density of states at the Fermi level expressed by an effective coupling parameter)[79] would restore spin-flip invariance for $\widetilde{B} = 0$ in the spin-dependent case and would thus erroneously imply $\langle \underset{\sim}{s}^z \rangle(\widetilde{B} = 0, T) = 0$. Instead, we are going to use NRG to determine the ELC field $\widetilde{B}_{\mathrm{ELC}}$ and to study the properties of $\underset{\sim}{H}_{\mathrm{eff}}^{(g_e=0)}(\widetilde{B}_{\mathrm{ELC}}; S, M)$.

For the interpretation of the properties of the full Hamiltonian (1) near the ELCs, we are going to use the main results for the effective model $\underset{\sim}{H}_{\mathrm{eff}}^{(g_e=0)}(\widetilde{B}_{\mathrm{ELC}}; S, M)$. These are explicitly demonstrated in Sec. VI B 4 and are summarized in the following. At an ELC, the spin-$\frac{1}{2}$ impurity of the effective model is Kondo screened for $T \to 0$. The temperature dependence of the impurity contribution to the entropy at an ELC is described by the corresponding universal function for the exchange-isotropic $S = \frac{1}{2}$ Kondo model without scattering term and Zeeman term. Since the parameters of the effective model are different near each free LC [see Eqs. (24) and (25)], there is also a different Kondo temperature T_K^{ELC} at each ELC. It turns out that T_K^{ELC} decreases with increasing M, i.e., T_K^{ELC} becomes smaller with every further ELC.

2. *Magnetic field dependence of impurity contributions near effective level crossing fields*

Armed with the effective model $\underset{\sim}{H}_{\mathrm{eff}}^{(g_e=0)}(\widetilde{B}; S, M)$ for a local magnetic field, we now study in detail the field dependence of typical impurity contributions of the full impurity model for moderately large anisotropy $D > 0$. In Fig. 9, results for $M_{\mathrm{imp}}(B)$, $S_{\mathrm{imp}}(B)$, and $T\chi_{\mathrm{imp}}(B)$ are shown for impurity spin $S = 3$ and anisotropy $D/W = 10^{-3}$. As before, equal g factors have been assumed.[80]

Let us start with a discussion of the magnetization curves depicted in Fig. 9(a). According to the previously considered behavior of the impurity magnetization $\mathcal{M}$ and its connection with M_{imp}, there are also steps in $M_{\mathrm{imp}}(B)$ at low temperature. These steps have finite widths for $T \to 0$ and are smeared out for sufficiently high temperature. It is noticeable that the steps have different widths: a step occurring at larger magnetic field is steeper. Figure 9(a) furthermore indicates that the effect of nonzero temperature is different for the different steps. In contrast, for a free spin with hard-axis anisotropy, the steps in the magnetization become discontinuous for $T \to 0$ and the effect of nonzero (small) temperature is the same for all of them (see Fig. 4). In the chosen representation of Fig. 9(a), the pseudoplateaux between the steps become flatter in the direction of increasing magnetic field and approach the true zero-temperature plateaux of the free spin with hard-axis anisotropy from below for growing D (cf. Fig. 5).

The behavior of $M_{\mathrm{imp}}(B)$ as shown in Fig. 9(a) can be understood by considering the magnetic field dependence of M_{imp} for the $S = \frac{1}{2}$ Kondo model with $g_e = g_S$. As discussed in Sec. IV A, $M_{\mathrm{imp}}(x, T = 0)$ is described by a universal function $f_{1/2}(x)$ with the variable $x = g_S\mu_B B/k_B T_H$ and $T_H \propto T_K$ according to Eq. (13).[46] $f_{1/2}(x)$ is linear in x for $x \ll 1$ and thus the slope of $M_{\mathrm{imp}}(B)$ for small fields is higher if the Kondo temperature is smaller.[46,47] This relation is also expressed by the definition of the Kondo temperature from Eq. (12). Combined with the prediction of the effective model with $g_e = 0$ for the Kondo temperatures at the different ELCs, this observation explains why different steps in a single magnetization curve of the full model have different widths at zero temperature. In case of the $S = \frac{1}{2}$ Kondo model, temperature has to reach the scale of T_K to become relevant for the zero-field susceptibility.[16] For this reason, thermal broadening of a step in $M_{\mathrm{imp}}(B)$ begins at lower temperature if the step occurs at a later ELC with smaller T_K^{ELC}. Furthermore, away from an ELC, the magnetization reaches values of the order of the respective saturation value for smaller magnetic fields (relative to the ELC field) if the Kondo temperature at the ELC is lower. It subsequently enters the regime of very slow growth towards saturation, which shows up in Fig. 9(a) in the form of a pseudoplateau. This also explains why pseudoplateaux between later ELCs with smaller T_K^{ELC} are flatter.

Results for the impurity contribution to the entropy $S_{\mathrm{imp}}(B)$ and the effective moment $T\chi_{\mathrm{imp}}(B)$ at low temperature $k_B T < D$ are shown in Figs. 9(b) and 9(c), respectively. In both cases, we observe peaks of varying height and width whose positions coincide with those of the steps in $M_{\mathrm{imp}}(B)$. We find that the peaks become both higher and narrower with every further ELC. If the temperature is reduced, the peak heights decline and at the same time, if T is not too low, the peaks become sharper. It is noticeable that there is a temperature below which the width of the first peak in both S_{imp} and $T\chi_{\mathrm{imp}}$ varies only little as a function of T.

At zero temperature, both S_{imp} and $T\chi_{\mathrm{imp}}$ vanish for all magnetic fields. In case of the entropy, the reason is that the magnetic field either leads to a nondegenerate ground state or it creates an effective impurity doublet which is then Kondo screened. The effective moment, on the other hand, has to go to zero since the slope of $M_{\mathrm{imp}}(B)$ at zero temperature, i.e., $\chi_{\mathrm{imp}}(B, T = 0)$, is finite for all fields. For large anisotropy D, the temperature dependence of the peak heights is determined by the pseudo-spin-$\frac{1}{2}$ Kondo effects that take place at the ELCs (see the next section and Fig. 10 for details). By recollecting results for the $S = \frac{1}{2}$ Kondo model,[51] we can furthermore understand the different peak widths and their temperature dependence. In case of the $S = \frac{1}{2}$ Kondo effect, the Zeeman energy $g_S\mu_B B$ has to reach the energy scale of $\max(k_B T, k_B T_H)$ in order to considerably suppress S_{imp} and $T\chi_{\mathrm{imp}}$.[51] In particular, since the lowest temperatures considered in Fig. 9 are smaller than T_K^{ELC} at the first ELC [cf. the indicated temperature range in Fig. 10(a)], temperatures are reached for which the thermal broadening of the first peak is small.

3. *Temperature dependence of impurity contributions at effective level crossing fields*

Figure 10 shows the temperature dependence of S_{imp}, $T\chi_{\mathrm{imp}}$, and χ_{imp} at the three ELCs that occur for the example considered in Fig. 9. In case of entropy and effective moment, it is thus demonstrated how the peak heights in Figs. 9(b) and 9(c) decrease when the temperature is lowered. Note

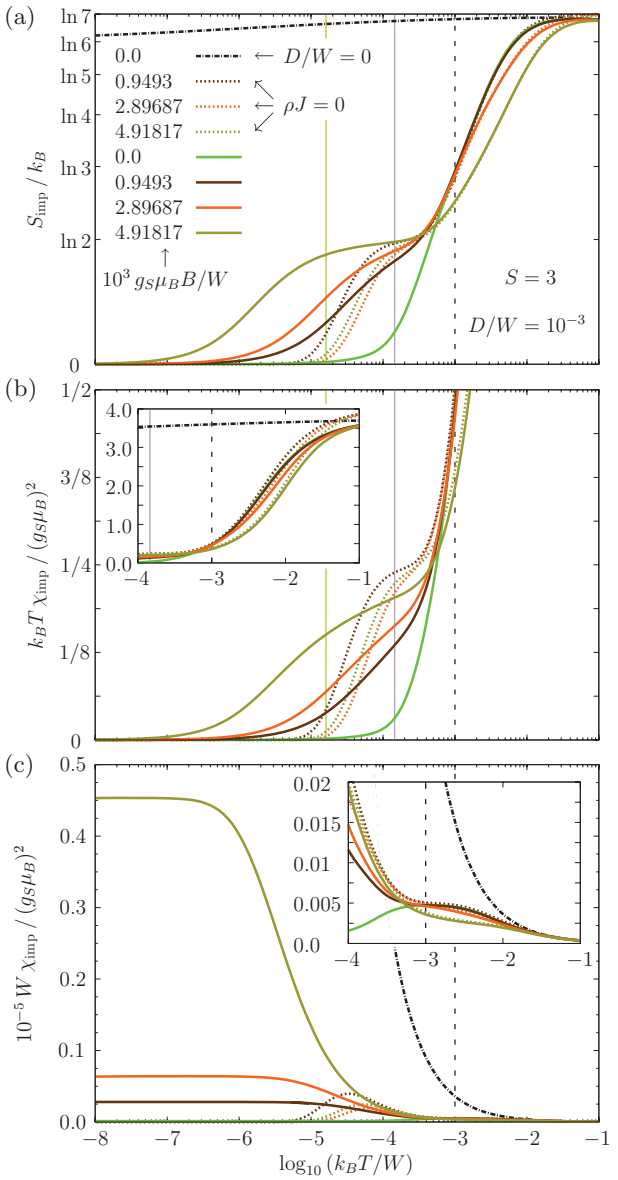

FIG. 10. (Color online) Main plots: Impurity contribution to (a) the entropy $S_{\rm imp}$, (b) the effective moment $T\chi_{\rm imp}$, and (c) the magnetic susceptibility $\chi_{\rm imp}$ as a function of temperature for impurity spin $S = 3$ and hard-axis anisotropy $D/W = 10^{-3}$. The chosen nonzero magnetic fields correspond to the peak positions for $S_{\rm imp}(B)$ and $T\chi_{\rm imp}(B)$ according to Fig. 9. Also shown are NRG results for vanishing coupling strength (dashed lines) and for $D = 0$ (dashed-dotted lines). Solid vertical lines delimit the temperature range considered in Fig. 9, whereas dashed vertical lines indicate the thermal energy for which $k_BT = D$. In the insets, data from the main plots are presented for a reduced temperature range.

that in this section "anisotropic impurity" always means "exchange-isotropic impurity in the presence of hard-axis anisotropy."

$S_{\rm imp}(T, B = 0)$ for an impurity with $S = 3$ and $D = 0$ interpolates between the limiting values of $k_B \ln 7$ (for $T \to \infty$) and $k_B \ln 6$ (for $T = 0$), according to the screening of half a magnetic moment [cf. Fig. 10(a)]. In contrast, for the anisotropic impurity in zero field, all higher-lying impurity levels are frozen out on the energy scale $k_BT \approx D$ so that $S_{\rm imp}(T, B = 0)$ quickly drops to zero.[63] At high temperatures $k_BT \gg D$, on the other hand, the anisotropic impurity behaves more and more like an impurity with $D = 0$. For the three ELC fields, we observe qualitatively different behavior at low temperature $k_BT < D$ compared to the case of zero field: Starting with $S_{\rm imp} \approx k_B \ln 2$ for $k_BT \lesssim D$, the effective impurity doublet, which is formed due to the magnetic field, undergoes Kondo screening with a value of $T_K^{\rm ELC}$ that decreases with every further ELC. While there is fair agreement with the results for a decoupled impurity at $k_BT > D$, low temperature $k_BT \ll D$ reveals that the ELC fields are not equal to the free LC fields. For this reason, all states except the respective nondegenerate ground state are ultimately frozen out for $T \to 0$.

For an impurity with $S = 3$ and $D = 0$, $k_BT\,\chi_{\rm imp}(T, B = 0)/(g_S\mu_B)^2$ obeys a Curie law at both high and low temperatures [see Fig. 10(b)] and goes from $S(S + 1)/3 = 4$ (for $T \to \infty$) to $(S - \frac{1}{2})(S + \frac{1}{2})/3 = 35/12$ (for $T = 0$). For the anisotropic impurity in zero magnetic field, on the other hand, the increasing thermal reduction to a nonmagnetic ground state for $k_BT < D$ leads to a vanishing effective moment at zero temperature.[63] At very high temperature $k_BT \lesssim W$ (not shown), we find the expected agreement between $T\chi_{\rm imp}(B = 0)$ for $D = 0$ and for $D > 0$. The effective moment of the decoupled anisotropic impurity first goes to about $\frac{1}{4}$ at $k_BT \lesssim D$ (according to the susceptibility of a doublet with $|\Delta M| = 1$), but then quickly drops to zero because of the nondegenerate ground state with good magnetic quantum number. For the anisotropic impurity at the ELC fields, we again observe Kondo screening for $T \to 0$ with different $T_K^{\rm ELC}$, starting with an effective moment of $k_BT\,\chi_{\rm imp}/(g_S\mu_B)^2 \approx \frac{1}{4}$ at $k_BT \lesssim D$.

According to its definition, the impurity contribution to the susceptibility $\chi_{\rm imp}$, for which results are presented in Fig. 10(c), is the slope of $M_{\rm imp}(B)$ and thus directly yields information about the width of the steps in the magnetization curve shown in Fig. 9(a). For an impurity with $D = 0$ and $S \geqslant 1$, the zero-field susceptibility at low temperature is described by a Curie law and thus diverges for $T \to 0$. In contrast, $\chi_{\rm imp}(T, B = 0)$ for the anisotropic impurity has a maximum at $k_BT \approx D$ and vanishes for zero temperature. Since the ELCs lie close to the free LCs in this example, the susceptibility for the decoupled anisotropic impurity displays a maximum at a thermal energy of the order of the level splitting, but then falls off at low temperature. At the ELCs, $\chi_{\rm imp}(T)$ for the anisotropic impurity saturates at a finite value for $T \to 0$ that increases with decreasing Kondo temperature. Recently, it has been demonstrated that a field-induced Kondo effect also occurs for Hamiltonian (1) with easy-axis anisotropy $D < 0$, additional transverse anisotropy E, and a local magnetic field aligned along the x axis.[65]

4. *Properties of the effective model for vanishing electron g factor*

We now return to the effective model for $g_e = 0$ given by Hamiltonian (30) in order to study its properties in greater detail. The ELC field $\widetilde{B}_{\rm ELC}$ and the Kondo temperature $T_K^{\rm ELC}$ *at the ELC field* are determined as a function of the parameters $J_\parallel$, $J_\perp$, and κ of the effective model or, respectively, as a function of the parameters J, S, and M of the full Hamiltonian

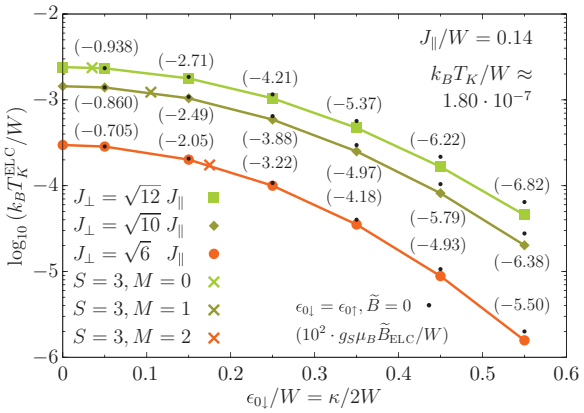

FIG. 11. (Color online) Kondo temperature at the ELC field (cf. Appendix D) for the effective Hamiltonian with $g_e = 0$ as a function of the scattering parameter κ (corresponding to a pair of onsite energies $\epsilon_{0\downarrow} = -\epsilon_{0\uparrow} > 0$ for the zeroth site of the Wilson chain) for fixed $J_\parallel$ and three values of the coupling parameter $J_\perp > J_\parallel$. Numbers in parentheses denote the respective ELC field and lines are intended as a guide to the eye. Pessimistic error bars would be smaller than the symbol size. Additional crosses indicate the Kondo temperature for parameters which, according to Eqs. (24) and (25), correspond to the given values of the quantum numbers S and M. Small dots mark T_K for the case of potential scattering, i.e., for spin-independent onsite energies *and zero magnetic field*. The Kondo temperature given in the upper right corner refers to the exchange-isotropic case without scattering term.

[according to Eqs. (24) to (26)]. In Appendix D, it is described how to reliably extract these quantities from the NRG results.

We first investigate how the parameter κ, which corresponds to spin-dependent scattering at the zeroth site of the Wilson chain with onsite energies $\epsilon_{0\downarrow} = -\epsilon_{0\uparrow} > 0$ as seen from Eqs. (22) and (24), affects the values of $\widetilde{B}_{\mathrm{ELC}}$ and T_K^{ELC}. To this end, we interpret κ as a free parameter of the effective model. For the exchange-isotropic $S = \frac{1}{2}$ Kondo model in zero magnetic field, it is known that ordinary (spin-independent) potential scattering can be approximately mapped to a modified electron DOS at the Fermi level or, equivalently, to an effective coupling parameter J_{eff}.[79] This approximation predicts that an increase of the scattering parameter reduces J_{eff} and thus also the Kondo temperature.

In the example shown in Fig. 11, spin quantum number $S = 3$ (as in Fig. 9) is considered and those coupling parameters $J_\perp$ are chosen which, as per Eq. (25), are assigned to the three magnetic quantum numbers allowed for this value of S (i.e., $M = 0,1,2$). Without scattering term, the Kondo temperature decreases when $J_\perp$ is reduced.[10,63] Additional spin-dependent scattering further lowers T_K^{ELC} just as standard potential scattering with $\epsilon_{0\downarrow} = \epsilon_{0\uparrow}$ at zero magnetic field does, but in comparison leads to smaller values of the Kondo temperature. In accordance with the expression for J_{eff} from Ref. 79, the sign of the spin-*independent* onsite energies does not affect T_K. Figure 11 reveals that the decrease of T_K^{ELC} accelerates with growing scattering strength. Furthermore, we observe that the spin-dependent scattering has a larger influence on the Kondo temperature at the ELC field when the coupling parameter $J_\perp$ is smaller.

Let us now turn to the effect of κ on the position of the ELC field. An additional spin-dependent scattering term breaks the spin-flip invariance and is therefore the very reason for a nonzero value of $\widetilde{B}_{\mathrm{ELC}}$. It thus seems plausible that a larger value of κ also leads to a larger absolute value of the ELC field (cf. the numbers in parentheses in Fig. 11). This increase of $|\widetilde{B}_{\mathrm{ELC}}|$ decelerates with growing scattering strength. A closer look at the data reveals that κ again has a stronger effect when the coupling parameter $J_\perp$ is smaller.

Additional crosses in Fig. 11 mark the Kondo temperature for those values of the scattering parameter κ that follow from Eq. (24) for the three considered M quantum numbers. We observe that the effective model predicts a decrease of T_K^{ELC} with growing M, i.e., with every further ELC. As the example demonstrates, this decline of the Kondo temperature is due to three cooperating effects: (1) According to Eq. (25), $J_\perp$ becomes smaller when M is increased. (2) Simultaneously, κ becomes larger. (3) Because of the decreasing value of $J_\perp$, the scattering parameter additionally gains in importance. For the ELC fields $g_S\mu_B\widetilde{B}_{\mathrm{ELC}}/W$ that belong to the three special values of T_K^{ELC}, we obtain the following results (the error estimates indicate the variance with respect to z, see Appendix D): $-6.59^{+0.19}_{-0.25} \times 10^{-3} (S = 3, M = 0)$, $-1.78^{+0.06}_{-0.07} \times 10^{-2}$ $(M = 1)$, and $-2.36^{+0.06}_{-0.09} \times 10^{-2}$ $(M = 2)$.

Finally, we investigate how the ELC field and the Kondo temperature at the ELC field depend on the parameters of the full Hamiltonian (1), i.e., on J, S, and M, with the parameters of the effective model given by Eqs. (24) to (26). First of all, we note that all obtained (relative) ELC fields are negative. This supports the conclusion that, in the impurity magnetization curves for equal g factors and large hard-axis anisotropy presented in Fig. 5, the free LC fields are only exceeded because of the electrons' nonzero magnetic coupling. For $S = 1$, $\frac{3}{2}$, 2 and $J/W = 0.14$ (as in Fig. 5), the following values for $g_S\mu_B\widetilde{B}_{\mathrm{ELC}}/W$ are obtained: $-3.90^{+0.10}_{-0.14} \times 10^{-3}$ $(S = 1, M = 0)$, $-8.27^{+0.22}_{-0.30} \times 10^{-3}$ $(S = \frac{3}{2}, M = \frac{1}{2})$, $-4.95^{+0.14}_{-0.18} \times 10^{-3}$ $(S = 2, M = 0)$, and $-1.31^{+0.04}_{-0.05} \times 10^{-2}$ $(S = 2, M = 1)$.

In contrast to the prediction of the effective model with $g_e > 0$ from Eq. (29), the ELC fields depend on the quantum numbers S and M for vanishing electron g factor (see Fig. 12). With increasing value of S, i.e., with increasing coupling parameter $J_\perp$, the absolute value of the ELC field grows as already seen in Fig. 11. A larger coupling J increases all parameters of the effective model ($J_\parallel, J_\perp$, and κ) and, as demonstrated by Fig. 12, thereby leads to a larger value of $|\widetilde{B}_{\mathrm{ELC}}|$. It is furthermore evident that, with growing J, the quantum number S gains in importance: Fig. 12 shows that the "curves" for fixed coupling strength "fan out" for larger values of J. The dependence of the ELC field on the magnetic quantum number is the result of two counteracting effects: (1) A larger value of M leads to smaller coupling strength $J_\perp$ which, on its own, would lower $|\widetilde{B}_{\mathrm{ELC}}|$. (2) On the other hand, the scattering term becomes stronger with increasing M and would, on its own, enlarge $|\widetilde{B}_{\mathrm{ELC}}|$. For the parameters considered in Fig. 12, there is a growth of $|\widetilde{B}_{\mathrm{ELC}}|$ with M for $S \leqslant \frac{7}{2}$ that decelerates with increasing M. In the case of $S = 4$ and both $J/W = 0.16$ and $J/W = 0.18$, we observe a decrease of the absolute value of the ELC field in the last step.

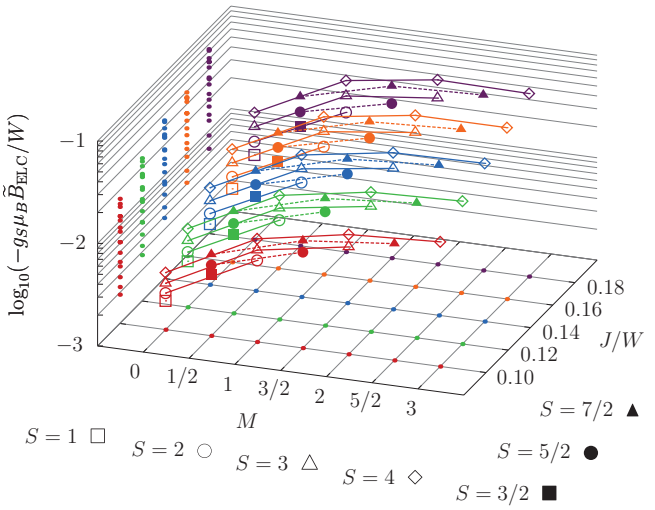

FIG. 12. (Color online) Negative value of the ELC field for a set of parameter combinations of the effective Hamiltonian with $g_e = 0$ which, according to Eqs. (24) to (26), correspond to the indicated spin quantum numbers S, magnetic quantum numbers $0 \leqslant M < S$, and coupling parameters J. Projections of the data points onto two planes are shown as small dots and lines connect points belonging to the same values of S and J. Pessimistic error bars would be smaller than the symbol size.

To conclude this section, the Kondo temperatures belonging to the ELC fields shown in Fig. 12 are presented in Fig. 13. As the main result, we find that, according to the above explanation, the value of $T_K^{\rm ELC}$ increasingly drops with growing M. On the other hand, a larger value of S increases the coupling strength $J_\perp$ and thus also $T_K^{\rm ELC}$. It turns out that the influence of S on $T_K^{\rm ELC}$ is reduced for larger coupling J.

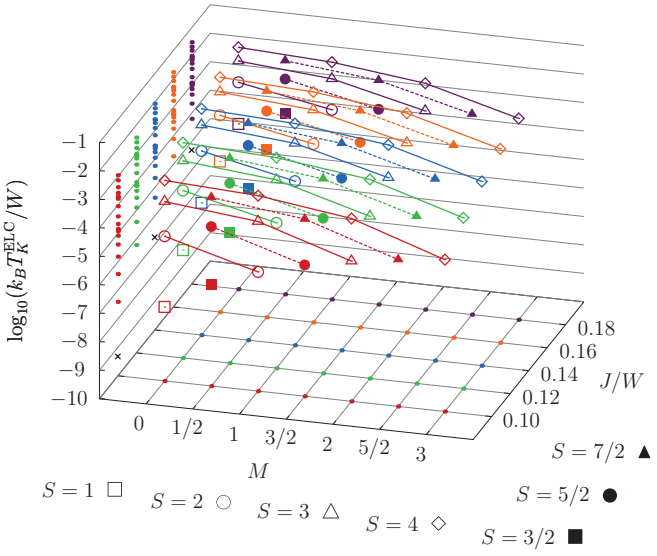

FIG. 13. (Color online) Kondo temperature at the respective ELC field for the same set of parameter combinations of the effective Hamiltonian with $g_e = 0$ as in Fig. 12. Again, pessimistic error bars would be smaller than the symbol size. Three small crosses in the plane spanned by $k_BT_K^{\rm ELC}/W$ and J/W indicate the value of the Kondo temperature for the exchange-isotropic case without scattering term [as inferred from Table I using Eq. (13)].

As a consequence, the "curves" for fixed J are "focused" in the direction of increasing coupling strength. We find that the dependence of the Kondo temperature on J is the result of two counteracting effects: (1) Both coupling parameters $J_\parallel$ and $J_\perp$ grow with J and would, on their own, lead to a larger value of $T_K^{\rm ELC}$. (2) However, the scattering parameter κ is also increased and would, on its own, lower the Kondo temperature. For all parameter combinations considered in Fig. 13, $T_K^{\rm ELC}$ is a monotonously increasing function of the coupling strength J. As a final observation, the relative decrease of the Kondo temperature between two consecutive values of M (for fixed J) becomes smaller for larger quantum number S.

5. *Comparison of anisotropy- and field-induced pseudo-spin-$\frac{1}{2}$ Kondo effect for half-integer impurity spin*

In the case of half-integer impurity spin $S \geqslant \frac{3}{2}$, two different pseudo-spin-$\frac{1}{2}$ Kondo effects occur for large hard-axis anisotropy D. At zero magnetic field, the anisotropy splits up the impurity multiplet and a doublet with magnetic quantum numbers $M = \pm\frac{1}{2}$ becomes the lowest-lying impurity level [cf. Fig. 4(b)]. If the energy gap to the impurity states with $M = \pm\frac{3}{2}$, which is equal to $2D$, is sufficiently large, this doublet undergoes pseudo-spin-$\frac{1}{2}$ Kondo screening (let us call this Kondo effect "anisotropy induced").[63] At nonzero magnetic field, on the other hand, ELCs with associated field-induced Kondo effects occur, as discussed in the previous section. Both types of Kondo effect show up in the corresponding impurity magnetization curves. In Fig. 7(a), for example, we observe the magnetic response of the effective impurity doublet at low magnetic fields $g_S\mu_BB/D \ll 1$, which is then followed by a step at $g_S\mu_BB/D \approx 2$ due to the ELC.

One might wonder how the Kondo temperatures of the anisotropy- and field-induced Kondo effects compare. It has been shown in Ref. 63 that the anisotropy-induced Kondo screening in the limit $D/W \to \infty$ is explained by Hamiltonian (30) with $\widetilde{B} = 0$ and parameters $J_\parallel = J$, $J_\perp^D = (S + \frac{1}{2})J$, and $\kappa = 0$. On the other hand, for $g_e = 0$ the pseudo-spin-$\frac{1}{2}$ Kondo effect at the first ELC (i.e., for $M = \frac{1}{2}$) is described by the same Hamiltonian with $\widetilde{B} = \widetilde{B}_{\rm ELC}$ and parameters $J_\parallel = J$, $J_\perp^{\rm ELC} = \sqrt{(S - \frac{1}{2})(S + \frac{3}{2})}\,J$, and $\kappa = J$. In particular, we thus have $J_\perp^{\rm ELC} < J_\perp^D$ for $S \geqslant \frac{3}{2}$. Since Fig. 11 shows that additional scattering κ reduces the Kondo temperature, we can conclude that T_K^D for the anisotropy-induced Kondo effect is always larger than $T_K^{\rm ELC}$ at the first ELC and, according to Fig. 13, at all following ELCs, too.

VII. SUMMARY

In this paper, we have reported on numerical renormalization group (NRG) calculations for a Kondo model with additional uniaxial anisotropy D. Results have been presented for nonzero magnetic field B and different ratios g_e/g_S of electron and impurity g factor.

For a bulk field (i.e., for equal g factors), a comparison of NRG results for the impurity magnetization $\mathcal{M}$ and the impurity contribution to the magnetization $M_{\rm imp}$ reveals that $\mathcal{M}(T,B) = \alpha M_{\rm imp}(T,B)$ as long as all relevant energy scales (i.e., thermal energy, Zeeman energy, and uniaxial anisotropy

according to Appendix C) are small compared to the half-bandwidth W. The proportionality factor $\alpha > 1$ depends on the coupling strength and decreases for smaller couplings $\rho J_\parallel$ and $\rho J_\perp$ as shown in Appendix C. Calculations for isotropic exchange interaction (i.e., $J_\parallel = J_\perp = J$) discussed in Appendix C demonstrate that, compared to the case of a local field (i.e., $g_e = 0$), a nonzero electron g factor effectively rescales the magnetic field argument of the impurity magnetization $\mathcal{M}(B)$ at low temperature. They furthermore suggest that the corresponding values of the rescaling factor $\eta(g_e/g_S = 1)$ and the proportionality factor α coincide. The results for $\mathcal{M}$ and M_{imp} mean that for a bulk field the magnetization of the conduction electrons is reduced due to the presence of the impurity spin and that a nonzero magnetic coupling of the electrons causes the impurity to effectively "feel" a reduced magnetic field strength. In particular, for an isotropic impurity ($D = 0$) in a bulk field, the calculations thus explicitly demonstrate that $\mathcal{M}(B,T \approx 0)$, unlike M_{imp}, does not display universal behavior in the usual sense as already noted in Ref. 49 (see also Appendix B).

With additional easy-axis anisotropy ($D < 0$), $M_{\text{imp}}(B,T \approx 0)$ starts to deviate from the curve for $D = 0$ at $g_S\mu_B B \approx |D|$ and stabilizes at a D-dependent value for small, but nonzero, magnetic field $g_S\mu_B B \ll |D|$. This ground-state magnetization matches the effective moment of the respective "fractional spin"[63] as given by $k_B T\,\chi_{\text{imp}}(B = 0)$ for $k_B T \ll |D|$. The magnetic response at small fields and low temperature (compared to $|D|$) is thus shown to resemble that of an ordinary magnetic doublet. Appropriately, the impurity magnetization $\mathcal{M}(B,T > 0)$ is well described by a rescaled and shifted Brillouin function in this regime.

In the case of hard-axis anisotropy ($D > 0$), a nonzero magnetic field can lead to "effective level crossings" (ELCs), at which pseudo-spin-$\frac{1}{2}$ Kondo screening occurs. For $g_e = 0$ and $D/W \to \infty$, these field-induced Kondo effects are described by an exchange-anisotropic spin-$\frac{1}{2}$ Kondo model with additional spin-dependent scattering at the zeroth site of the Wilson chain. At the respective ELC field, this scattering leads to a reduction of the Kondo temperature T_K^{ELC} in a similar way as ordinary potential scattering does for zero magnetic field. In particular, the effective model predicts that T_K^{ELC} decreases with every further ELC. This agrees with the observation that the steps in the magnetization curves for large D, which are due to the field-induced Kondo effects, become steeper in the direction of increasing magnetic field. We furthermore find that the step positions are shifted relative to the level crossing fields of the corresponding free spin with hard-axis anisotropy (this is either a spin S if D is much larger than the energy scale $k_B T_H$ or a spin $S - \frac{1}{2}$ if $D/k_B T_H \ll 1$) and, in particular, that they are also influenced by a nonzero magnetic coupling of the conduction electrons.

ACKNOWLEDGMENTS

We thank T. Pruschke and S. Schmitt for helpful discussions. In particular, we would like to thank T. Costi for lots of valuable advice and for carefully reading and critically commenting on the manuscript. Part of the calculations presented in this paper have been done at the Leibniz-Rechenzentrum (LRZ) in Garching near Munich. Financial support by the Deutsche Forschungsgemeinschaft (DFG) through research group FOR 945 is gratefully acknowledged.

APPENDIX A: NUMERICAL RENORMALIZATION GROUP CALCULATIONS WITH CONDUCTION ELECTRON ZEEMAN TERM

In this first Appendix, we briefly describe the changes to the standard NRG procedure[18] which are necessary in order to carry out calculations with an additional Zeeman term for the conduction electrons.

1. Logarithmic discretization

The starting point is the continuous energy representation of the Hamiltonian from Eq. (8) with a restriction to the physically reasonable case $h < W$. In the following, it is assumed that the magnetic field, which appears in $h = g_e\mu_B B$, is nonzero and fixed and, to simplify the notation, that the chemical potential is zero. We introduce abbreviations for the absolute value of the integration boundaries in Eq. (8),

$$\mathcal{B}_\mu^\pm = |\pm W + \mu h|, \tag{A1}$$

rescale the integration variable ε, and change to rescaled electron operators (cf. Ref. 17)

$$\xi_\mu^+ = \frac{\varepsilon}{\mathcal{B}_\mu^+} \quad \text{for} \quad \varepsilon > 0, \tag{A2}$$

$$\xi_\mu^- = \frac{\varepsilon}{\mathcal{B}_\mu^-} \quad \text{for} \quad \varepsilon < 0, \tag{A3}$$

$$\underset{\sim}{a}_{\xi\mu}^+ = \sqrt{\mathcal{B}_\mu^+}\,\underset{\sim}{a}_{\varepsilon\mu} \quad \text{for} \quad \varepsilon > 0, \tag{A4}$$

$$\underset{\sim}{a}_{\xi\mu}^- = \sqrt{\mathcal{B}_\mu^-}\,\underset{\sim}{a}_{\varepsilon\mu} \quad \text{for} \quad \varepsilon < 0. \tag{A5}$$

Using $\int_{-W}^{W} d\varepsilon\,\rho(\varepsilon) = 1$ and defining the normalized zeroth state of the Wilson chain as

$$\underset{\sim}{f}_{0\mu} = \int_0^1 d\xi_\mu^+ \sqrt{\rho(\xi_\mu^+\mathcal{B}_\mu^+ - \mu h)\mathcal{B}_\mu^+}\,\underset{\sim}{a}_{\xi\mu}^+ + \int_{-1}^0 d\xi_\mu^- \sqrt{\rho(\xi_\mu^-\mathcal{B}_\mu^- - \mu h)\mathcal{B}_\mu^-}\,\underset{\sim}{a}_{\xi\mu}^-, \tag{A6}$$

we obtain an equivalent expression for the electronic and interaction term in Eq. (8):

$$\underset{\sim}{H}_{\text{cb+int}} = W\sum_\mu \left(\frac{\mathcal{B}_\mu^+}{W}\int_0^1 d\xi_\mu^+\,\xi_\mu^+\,\underset{\sim}{a}_{\xi\mu}^{+\dagger}\underset{\sim}{a}_{\xi\mu}^+ + \frac{\mathcal{B}_\mu^-}{W}\int_{-1}^0 d\xi_\mu^-\,\xi_\mu^-\,\underset{\sim}{a}_{\xi\mu}^{-\dagger}\underset{\sim}{a}_{\xi\mu}^- \right) + J\,\underset{\sim}{\boldsymbol{S}}\cdot\sum_{\mu,\nu}\underset{\sim}{f}_{0\mu}^\dagger\frac{\boldsymbol{\sigma}_{\mu\nu}}{2}\underset{\sim}{f}_{0\nu}. \tag{A7}$$

Next, the logarithmic discretization of the conduction band is carried out according to one of the available discretization schemes[70,71,81–84] by dividing the integration range $[-1,1]$ into standard intervals $I_m^\pm$ and using the following weight function on the mth positive and negative intervals, respectively:

$$\varphi_{m\mu}^\pm(\xi_\mu^\pm) = \sqrt{\frac{\rho(\xi_\mu^\pm\mathcal{B}_\mu^\pm - \mu h)}{\int_{I_m^\pm} d\xi_\mu'^\pm\,\rho(\xi_\mu'^\pm\mathcal{B}_\mu^\pm - \mu h)}}. \tag{A8}$$

With $s = \pm$,

$$\gamma^s_{m\mu} = \sqrt{\frac{\mathcal{B}^s_\mu}{W} \int_{I^s_m} d\xi^s_\mu \, \rho\big(\xi^s_\mu \mathcal{B}^s_\mu - \mu h\big) W}, \tag{A9}$$

and new operators $\underset{\sim}{a}^s_{m\mu}$ corresponding to the weight functions $\varphi^s_{m\mu}(\xi^s_\mu)$ on the intervals I^s_m, we have the following exact representation for the zeroth state of the Wilson chain:

$$\underset{\sim}{f}_{0\mu} = \sum_{s,m} \gamma^s_{m\mu} \, \underset{\sim}{a}^s_{m\mu}. \tag{A10}$$

In addition, a "dimensionless energy" $\mathcal{E}^s_{m\mu}$ has to be assigned to each interval I^s_m for each spin projection μ. This is done according to the chosen discretization scheme by using the weight function (A8) with the shifted DOS, leading to a discrete approximation to Hamiltonian (A7):

$$\begin{aligned} \underset{\sim}{H}_{\text{cb+int}} \to W \sum_{s,m,\mu} \frac{\mathcal{B}^s_\mu}{W} \mathcal{E}^s_{m\mu} \, \underset{\sim}{a}^{s\dagger}_{m\mu} \, \underset{\sim}{a}^s_{m\mu} \\ + J \, \underset{\sim}{\boldsymbol{S}} \cdot \sum_{\mu,\nu} \underset{\sim}{f}^\dagger_{0\mu} \frac{\boldsymbol{\sigma}_{\mu\nu}}{2} \underset{\sim}{f}_{0\nu}. \end{aligned} \tag{A11}$$

At this point, the substitution (A11) is still valid for arbitrary $\rho(\varepsilon)$. The above expressions simplify in the case of a constant density of states, $\rho(\varepsilon) = 1/2W$, as a shifted constant DOS is, of course, still a constant DOS:

$$\begin{aligned} \underset{\sim}{H}_{\text{cb+int}} \to W \sum_{s,m,\mu} \frac{\mathcal{B}^s_\mu}{W} \underbrace{\mathcal{E}^s_{m\mu}(h=0)}_{=\mathcal{E}^s_m} \underset{\sim}{a}^{s\dagger}_{m\mu} \, \underset{\sim}{a}^s_{m\mu} \\ + J \, \underset{\sim}{\boldsymbol{S}} \cdot \sum_{\mu,\nu} \underset{\sim}{f}^\dagger_{0\mu} \frac{\boldsymbol{\sigma}_{\mu\nu}}{2} \underset{\sim}{f}_{0\nu}, \end{aligned} \tag{A12}$$

$$\underset{\sim}{f}_{0\mu} = \sum_{s,m} \sqrt{\frac{\mathcal{B}^s_\mu}{W}} \underbrace{\gamma^s_{m\mu}(h=0)}_{=\gamma_m} \underset{\sim}{a}^s_{m\mu}. \tag{A13}$$

Here, $\mathcal{E}^s_m$ and γ_m are the "energies" and expansion coefficients, respectively, for the system with a *local* magnetic field (i.e., with $g_e = 0$).

2. Tridiagonalization

Since the rescaling factors

$$\frac{\mathcal{B}^s_\mu}{W} = \left| s + \mu \frac{g_e}{g_S} \frac{g_S \mu_B B}{W} \right| \tag{A14}$$

depend on spin projection μ and magnetic field B, the tridiagonalization of Hamiltonian (A12), which leads to the Wilson chain with hopping parameters $t_{i\mu}(B)$ and onsite energies $\epsilon_{i\mu}(B)$, has to be done separately for spin up and spin down and for each value of B. In case of a constant DOS, Eqs. (A12) and (A13) show that the only necessary modification of an existing code solving the recursion relations given in Ref. 18 is to multiply all "energies" $\mathcal{E}^s_m$ and coefficients γ^2_m with the appropriate factor (A14).

For a particle-hole symmetric DOS, we have $\mathcal{E}^s_{m\mu} = -\mathcal{E}^{-s}_{m-\mu}$ and $\gamma^s_{m\mu} = \gamma^{-s}_{m-\mu}$. Using the ansatz $u_{nm\mu} = (-1)^n v_{nm-\mu}$ and $v_{nm\mu} = (-1)^n u_{nm-\mu}$ for the coefficients of the orthogonal transformation (following the notation of Ref. 18), it can then be shown that $t_{i\uparrow}(B) = t_{i\downarrow}(B)$ and $\epsilon_{i\uparrow}(B) = -\epsilon_{i\downarrow}(B)$ for all sites i of the Wilson chain.

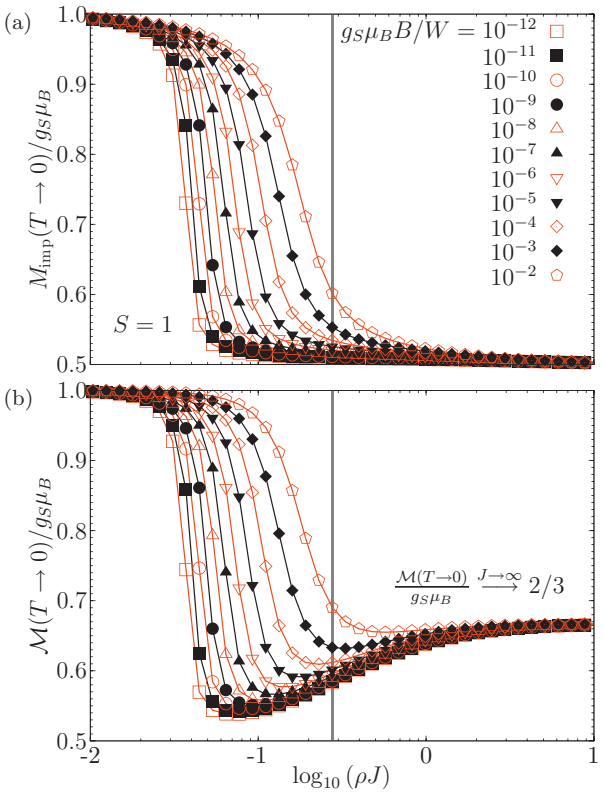

FIG. 14. (Color online) Limiting value for $T \to 0$ of (a) the impurity contribution to the magnetization M_{imp} and (b) the impurity magnetization $\mathcal{M}$ as a function of the coupling strength ρJ for impurity spin $S = 1$, $g_e = g_S$, and several magnetic field values. The vertical lines mark a coupling strength of $\rho J' \approx 0.276$ for which we have checked by comparing with the respective Bethe ansatz solution shown in Fig. 1 that $M_{\text{imp}}(B, T \approx 0)$ still exhibits universal behavior (a fit of the BA curve gives $k_B T_H / W \approx 8.85 \times 10^{-2}$). Remaining lines are intended as a guide to the eye.

APPENDIX B: DEPENDENCE OF THE ZERO-TEMPERATURE MAGNETIZATION ON THE COUPLING STRENGTH FOR $D = 0$

To further illustrate the difference between the impurity contribution to the magnetization M_{imp} and the impurity magnetization $\mathcal{M}$ for vanishing anisotropy $D = 0$, we examine how both quantities depend on the coupling strength ρJ for nonzero magnetic field at zero temperature. As in Sec. IV, the case of equal g factors for impurity and electrons is considered. NRG results for impurity spin $S = 1$ and $\frac{3}{2}$ are shown in Figs. 14 and 15, respectively.

Let us begin the interpretation of the plots by considering the limiting cases $J \to 0$ and $J \to \infty$. For vanishing coupling strength, impurity and electrons are decoupled and thus both M_{imp} and $\mathcal{M}$ correspond to the magnetization of the respective free spin [cf. Eqs. (9) and (11)] which takes the value $g_S \mu_B S$ for any positive magnetic field at $T = 0$. However, the behavior in the limit $J \to \infty$ differs for the two quantities, again demonstrating that in general $M_{\text{imp}} \neq \mathcal{M}$. The values of M_{imp}

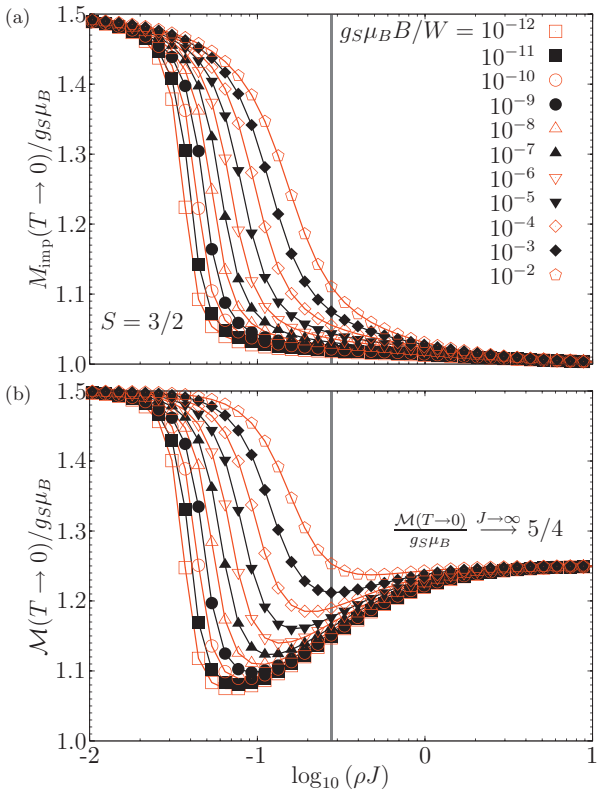

FIG. 15. (Color online) Limiting value for $T \to 0$ of (a) the impurity contribution to the magnetization and (b) the impurity magnetization as a function of the coupling strength ρJ as in Fig. 14, but here for impurity spin $S = \frac{3}{2}$. $M_{\rm imp}(B, T \approx 0)$ again shows universal behavior for $\rho J' \approx 0.276$ and a fit of the corresponding universal BA curve gives $k_B T_H / W \approx 3.05 \times 10^{-1}$.

and $\mathcal{M}$ in this limit can be understood by considering a simplified model: For very large values of J, it is energetically favorable that the lattice site the spin operator $\underset{\sim}{s}_0$ in Eq. (5) is associated with is singly occupied with a probability near one. We can then replace $\underset{\sim}{s}_0$ by a spin-$\frac{1}{2}$ operator $\underset{\sim}{s}$. Furthermore, all other terms in Hamiltonian (1) that involve degrees of freedom different from the impurity and the lattice site to which it couples can be neglected. We are thus left with a strongly coupled antiferromagnetic dimer in a magnetic field with Hamiltonian

$$\underset{\sim}{H}_{J\to\infty} = J\,\underset{\sim}{\boldsymbol{S}} \cdot \underset{\sim}{\boldsymbol{s}} + g_S\mu_B B(\underset{\sim}{S}^z + \underset{\sim}{s}^z). \tag{B1}$$

To determine the limiting value of $\mathcal{M}(T=0)/g_S\mu_B$ for $J \to \infty$ and any positive magnetic field, we have to calculate the expectation value of $-\underset{\sim}{S}^z$ with respect to that eigenstate of total spin which has the lowest value of $S_{\rm total}$ and corresponding z projection $M_{\rm total} = -S_{\rm total}$. Denoting eigenstates of Hamiltonian (B1) as $|S_{\rm total}, M_{\rm total}\rangle$, we find

$$-\langle 0,0|\underset{\sim}{S}^z|0,0\rangle = 0 \quad \text{for} \quad S = 1/2, \tag{B2}$$

$$-\left\langle \tfrac{1}{2},-\tfrac{1}{2}\middle|\underset{\sim}{S}^z\middle|\tfrac{1}{2},-\tfrac{1}{2}\right\rangle = \tfrac{2}{3} \quad \text{for} \quad S = 1, \tag{B3}$$

$$-\langle 1,-1|\underset{\sim}{S}^z|1,-1\rangle = \tfrac{5}{4} \quad \text{for} \quad S = 3/2. \tag{B4}$$

In contrast, in the limit $J \to \infty$ the impurity contribution to the magnetization $M_{\rm imp}(T=0)/g_S\mu_B$ for positive field reduces to $-\langle \underset{\sim}{S}^z + \underset{\sim}{s}^z \rangle$ with respect to the above eigenstates of Hamiltonian (B1). This expectation value gives $S - \frac{1}{2}$. The case $S = \frac{1}{2}$ is therefore special since both $M_{\rm imp}$ and $\mathcal{M}$ go to zero for $J \to \infty$. Figures 14 and 15 show that NRG, as a method that is nonperturbative in J, can in fact reproduce the limiting values for large coupling strength.[85]

Let us now consider the magnetization for intermediate values of ρJ. In the special case $S = \frac{1}{2}$, both $M_{\rm imp}$ and $\mathcal{M}$ are monotonically decreasing functions of the coupling strength for constant magnetic field B that show similar behavior. On the other hand, $M_{\rm imp}$ and $\mathcal{M}$ show a qualitatively different dependence on ρJ for impurity spin $S \geqslant 1$. While $M_{\rm imp}$ is again a monotonically decreasing function of the coupling strength for given magnetic field [see Figs. 14(a) and 15(a)], $\mathcal{M}(\rho J)$ displays a minimum for all considered values of B [cf. Figs. 14(b) and 15(b)].

It is instructive to compare the NRG results with the Bethe ansatz solution[46,47] for the field dependence of $M_{\rm imp}(T=0)$, given by the monotonically increasing universal function $f_S(x)$ (cf. Sec. IV A). According to the values reported in Table I and the standard estimate for the Kondo temperature from Eq. (14) for $S = \frac{1}{2}$, an increase of the coupling strength for constant magnetic field ought to lead to a larger scale $k_B T_H$ and hence to a lower rescaled field $x = g_S\mu_B B / k_B T_H$ and a smaller value of $M_{\rm imp}$. The impurity contribution to the magnetization for fixed positive field should therefore be a monotonically decreasing function of the coupling strength in the scaling regime. This conclusion is in line with the NRG results for $M_{\rm imp}(\rho J)$ shown in Figs. 14(a) and 15(a). The vertical lines in the plots mark a coupling strength $\rho J' \approx 0.276$, for which we have checked via a fit to the BA solution that $M_{\rm imp}(B, T \approx 0)$ still displays universal behavior. The scaling regime therefore extends at least up to coupling strengths as large as $\rho J'$ (apart from establishing this bound, the value of $\rho J'$ is arbitrary). In contrast, for low field the impurity magnetization $\mathcal{M}(\rho J)$ has a minimum for coupling strengths smaller than $\rho J'$ [cf. Figs. 14(b) and 15(b)]. We conclude that this behavior of $\mathcal{M}(\rho J)$ is not compatible with the standard scaling picture as described above for $M_{\rm imp}(\rho J)$.

APPENDIX C: EFFECT OF THE ELECTRON g FACTOR ON $\mathcal{M}$ AND THE CONNECTION BETWEEN $\mathcal{M}$ AND $M_{\rm imp}$

We now investigate how the impurity magnetization $\mathcal{M}(B, T \approx 0)$ is affected by a nonzero electron g factor corresponding to a positive ratio $g_e/g_S > 0$. Because of the sharp features that are found in the magnetization curves for $D > 0$ (see Fig. 5), the case of hard-axis anisotropy seems well suited to study the influence of nonzero g_e [alternatively, one could examine the effect of the electron g factor on the basis of the linear magnetic field dependence of $\mathcal{M}(B)$ for small B]. As an example, Fig. 16 shows magnetization curves $\mathcal{M}(B, T \approx 0)$ for impurity spin $S = 1$, moderately large D, and several g-factor ratios interpolating between a local field ($g_e = 0$) and a bulk field ($g_e = g_S$).

The results presented in Fig. 16 demonstrate that a positive electron g factor effectively causes a rescaling of the magnetic

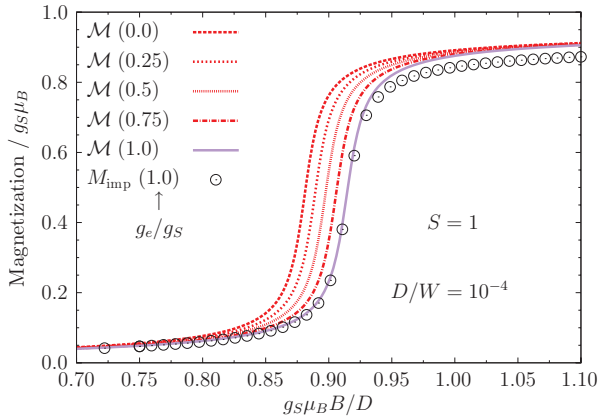

FIG. 16. (Color online) Impurity magnetization $\mathcal{M}$ as a function of magnetic field for impurity spin $S = 1$, hard-axis anisotropy $D/W = 10^{-4}$, coupling strength $\rho J = 0.07$, and several values of the g-factor ratio g_e/g_S [cf. Fig. 5(a) for $g_e = g_S$]. For equal g factors, the impurity contribution to the magnetization $M_{\rm imp}(B)$ is shown, too. The temperature is $k_BT/W \approx 1.54 \times 10^{-15} \approx 0$ in all cases.

field argument of the impurity magnetization: A ratio $g_e/g_S > 0$ shifts the impurity magnetization curve for $g_e = 0$ towards larger fields and thus reduces $\mathcal{M}(B,T \approx 0)$, which is a monotonically increasing function of B, for a fixed magnetic field value. Using the notation $\mathcal{M}(B,T,g_S,g_e)$, this statement can be expressed in the following way:

$$\mathcal{M}(B,T \approx 0,g_S,0) = \mathcal{M}(B',T \approx 0,g_S,g_e), \qquad \text{(C1)}$$

$$B' = \eta(\rho J,g_e/g_S)B, \qquad \text{(C2)}$$

with a rescaling factor $\eta(\rho J,g_e/g_S) \geqslant 1$ for $g_e/g_S \geqslant 0$ that depends on the coupling strength ρJ. Taking the magnetization curve for a local field as reference, we may therefore state that the impurity effectively "feels" a smaller magnetic field if there is also a Zeeman term for the electrons in Hamiltonian (1).

For a bulk field, Fig. 16 additionally shows the impurity contribution to the magnetization $M_{\rm imp}(B,T \approx 0)$ [according to Eq. (11), $\mathcal{M}$ and $M_{\rm imp}$ are equal for a local field]. We find that Eq. (15), which was obtained for $D = 0$, is also suitable to describe the relation between $\mathcal{M}(B,T \approx 0)$ and $M_{\rm imp}(B,T \approx 0)$ in the case of easy-axis and hard-axis anisotropy for magnetic fields $g_S\mu_B B \ll W$. A study of the connection between $\mathcal{M}$ and $M_{\rm imp}$ for $D < 0$ and $D > 0$ with $|D| \ll W$ reveals for impurity spin $S = 1$ and $\frac{3}{2}$ that the magnetic field averaged values for $\alpha(\rho J = 0.07)$ are nearly identical to the results for $D = 0$ reported in Table I, and that the standard deviations have the same order of magnitude. For $S = 2$, the obtained value of the proportionality factor is $\alpha(0.07) = 1.0370(1)$. We conclude that the effect of the uniaxial anisotropy on the value of α must be very small as long as $|D| \ll W$.

An analysis of the impurity magnetization curves for hard-axis anisotropy furthermore shows that the values of the rescaling factor $\eta(0.07,1)$ (approximately 1.038 for $S = 1$, 1.0375 for $S = \frac{3}{2}$, and 1.037 for $S = 2$) and the corresponding proportionality factor $\alpha(0.07)$ are remarkably similar. In the case of $S = 1$ and $D > 0$, we have also studied the difference between $\mathcal{M}(B,T \approx 0)$ for a local and bulk magnetic field for the two other coupling strengths previously considered (i.e., for $\rho J = 0.05$ and $\rho J = 0.09$). The rescaling factors obtained for $D \ll W$ [$\eta(0.05,1) \approx 1.0265$ and $\eta(0.09,1) \approx 1.0497$] are again in remarkable agreement with the corresponding values of $\alpha(\rho J)$. Moreover, we find that Eqs. (C1) and (C2), with the values of $\eta(\rho J,1)$ as determined for $D > 0$, are also suitable to describe the relation between the impurity magnetization curves for a local and bulk magnetic field for anisotropy $D \leqslant 0$. As $\mathcal{M}(B,T \approx 0)$ lacks sharp features in the $D = 0$ and easy-axis case, the effect of a nonzero electron g factor is more subtle, though.

The numerical results thus strongly suggest that the rescaling factor $\eta(\rho J,1)$ and the proportionality factor $\alpha(\rho J)$ take the same value. Furthermore, we find our results for the rescaling factor to be compatible with the conclusion of Ref. 49 that, in the case of the Kondo model with $S = \frac{1}{2}$, the g factor of the electrons (or equivalently their magnetic moment) is irrelevant for impurity properties in the limit of infinite bandwidth, corresponding to $\rho J \to 0$.

In the case of impurity spin $S = \frac{1}{2}$, it is possible to compare the obtained values for $\eta(\rho J,1)$ and $\alpha(\rho J)$ with previously published results. For the exchange-anisotropic multichannel $S = \frac{1}{2}$ Kondo model with transverse coupling strength $\rho J_\perp \ll 1$ [see Eq. (22) for the meaning of the symbols $J_\perp$ and $J_\parallel$], it is known that the impurity contributions to the free energy $F_{\rm imp}(B,T,g_S,g_e)$ for local and bulk magnetic fields have the following relation:[86]

$$F_{\rm imp}(B,T,g_S,g_S) = F_{\rm imp}(\bar{B},T,g_S,0), \qquad \text{(C3)}$$

$$\bar{B} = (1 - 2f\delta/\pi)B. \qquad \text{(C4)}$$

Here, f is the number of electron channels and δ is the phase shift generated by the longitudinal coupling $J_\parallel$. This result for $F_{\rm imp}$ is a generalization of the conclusion that the impurity contribution to the susceptibility $\chi_{\rm imp}(g_S,g_e)$ *at zero magnetic field* satisfies $\chi_{\rm imp}(g_S,g_e) = \lambda(g_e/g_S,\delta)\,\chi_{\rm imp}(g_S,g_S)$, with a certain factor λ, for the single-channel exchange-anisotropic $S = \frac{1}{2}$ Kondo model with $\rho J_\perp \ll 1$.[87] Using the definition for the impurity contribution to the magnetization $M_{\rm imp} = -\partial F_{\rm imp}/\partial B$ and the equivalence of $M_{\rm imp}$ and the impurity magnetization $\mathcal{M}$ for $g_e = 0$ according to Eq. (11), the following relation is obtained from Eqs. (C3) and (C4):

$$M_{\rm imp}(B,T,g_S,g_S) = (1 - 2f\delta/\pi)\,\mathcal{M}((1 - 2f\delta/\pi)B,T,g_S,0). \qquad \text{(C5)}$$

On the other hand, the proportionality $\mathcal{M}(B,T \approx 0,g_S,g_S) = \alpha(\rho J)M_{\rm imp}(B,T \approx 0,g_S,g_S)$ from Eq. (15) that is implied by the NRG results can be combined with Eqs. (C1) and (C2) to give

$$M_{\rm imp}(B,T \approx 0,g_S,g_S) = \frac{1}{\alpha(\rho J)}\,\mathcal{M}\left(\frac{B}{\eta(\rho J,1)},T \approx 0,g_S,0\right). \qquad \text{(C6)}$$

With $f = 1$ and the phase shift for the case of an electron band of width $2W$ with constant DOS $\rho = 1/2W$,[88] $\delta(\rho J_\parallel) =$

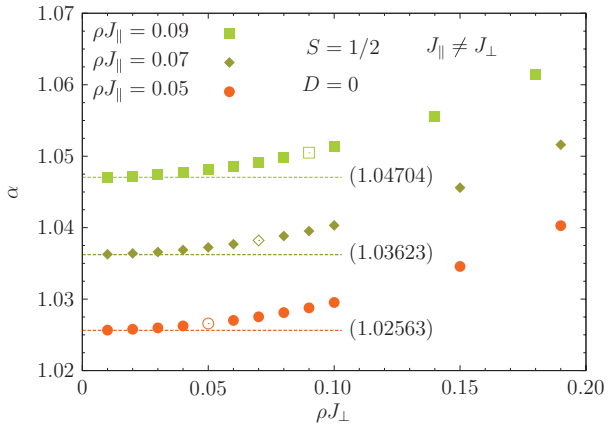

FIG. 17. (Color online) Proportionality factor α appearing in Eq. (15) as a function of the transverse coupling strength $\rho J_\perp$ for impurity spin $S = \frac{1}{2}$ and three values of the longitudinal coupling $\rho J_\parallel$. Dashed horizontal lines mark the values of α, given by the numbers in parentheses, that are predicted by Eq. (C7) for $\rho J_\perp \ll 1$. Open symbols indicate the proportionality factors for the exchange-isotropic case (i.e., $J_\parallel = J_\perp$), which are also found in Table I. As before, α has been averaged over magnetic fields $g_S\mu_B B/W \in [10^{-13}, 10^{-1}]$ for $k_BT/W \approx 1.54 \times 10^{-15} \approx 0$. The corresponding standard deviations would amount to error bars smaller than the symbol size.

arctan $(\pi\rho J_\parallel/4)$ (note the sign change with respect to Ref. 88), we compare Eqs. (C5) and (C6) and deduce for $\rho J_\perp \ll 1$

$$\alpha(\rho J_\parallel) = \eta(\rho J_\parallel, 1) = \frac{1}{1 - \frac{2}{\pi}\arctan(\pi\rho J_\parallel/4)}. \qquad \text{(C7)}$$

This equation predicts, in particular, that both the proportionality factor and the rescaling factor tend to 1 in the limit $\rho J_\parallel \to 0$. From Eq. (C7), the following values for $\alpha(\rho J_\parallel)$ are obtained: $\alpha = 1.02563$ $(\rho J_\parallel = 0.05)$, 1.03623 (0.07), and 1.04704 (0.09). In Fig. 17, we present NRG results for $\alpha(\rho J_\parallel, \rho J_\perp)$ for an impurity spin $S = \frac{1}{2}$ with exchange anisotropy. It is seen that the calculated proportionality factors indeed approach the predictions of Eq. (C7) for decreasing transverse coupling strength $\rho J_\perp$. For $\rho J_\perp = 0.01$ and all three considered values of $\rho J_\parallel$, the relative deviation is about 4×10^{-5}. In the exchange-isotropic case (i.e., $J_\parallel = J_\perp = J$), the relative deviation is less than half a percent, with better agreement for smaller coupling J.

Since Eqs. (C3) and (C4) also hold for nonzero temperature, the connection between $\mathcal{M}(B, T > 0)$ and $M_{\text{imp}}(B, T > 0)$ has been studied for impurity spin $S = \frac{1}{2}$, 1, and $\frac{3}{2}$ in the case of $D = 0$ and isotropic coupling $\rho J = 0.05, 0.07$, and 0.09. Keeping the coupling strength fixed, $\mathcal{M}(B, T)$ and $M_{\text{imp}}(B, T)$ are still proportional for nonzero temperature and it is found that, for $g_S\mu_B B/W \in [10^{-13}, 10^{-1}]$, the relative deviation between the proportionality factor and the corresponding value $\alpha(\rho J, T \approx 0)$ is less than 1‰ for thermal energies $k_BT/W \leqslant 10^{-2}$.

APPENDIX D: TECHNICAL DETAILS REGARDING THE STUDY OF THE EFFECTIVE MODEL FOR VANISHING ELECTRON g FACTOR

In this last Appendix, we describe how to reliably extract the ELC field $\widetilde{B}_{\text{ELC}}$ and the Kondo temperature T_K^{ELC} *at the ELC field* from the NRG results for the effective model (30) with $g_e = 0$.

To determine $\widetilde{B}_{\text{ELC}}$ as defined in Eq. (28), the impurity magnetization in units of $g_S\mu_B$ for the effective model $-\langle \underset{\sim}{s}^z\rangle(\widetilde{B})$ is calculated for low temperature $k_BT \ll W$. In the vicinity of an ELC, i.e., near its root, the impurity magnetization depends linearly on the (relative) magnetic field $\widetilde{B}$. The root, which corresponds to $\widetilde{B}_{\text{ELC}}$ at $T = 0$, can therefore be determined by performing a linear fit to the numerical data. However, the following complication arises: The position of the root of $\langle \underset{\sim}{s}^z\rangle(\widetilde{B})$ depends on the value of the twist parameter z and thereby on the discretization of the electron band. On the contrary, a physically meaningful result for the ELC field should display only a weak dependence on the numerical parameters of a NRG calculation in order to accurately reflect the continuum limit $\Lambda \to 1$. It turns out that a standard z averaging, i.e., an averaging of the impurity magnetization curves for different values of z at fixed temperature, is not reasonable at this point. Near an ELC, such an averaging in general introduces artifacts into the averaged curve because of nonlinear components which some of the z-dependent curves might already comprise. Similar numerical artifacts are found in the z-averaged magnetization curves of the full impurity model for large hard-axis anisotropy. Upon closer inspection, one discovers that z averaging divides the total height of a magnetization step into smaller "substeps" of equal height whose number corresponds to the number of z values used.

For the effective model with one set of parameters, the dependence of the impurity magnetization root on the discretization of the electron band is demonstrated in Fig. 18. There, the three common discretization schemes are compared for three different values of the discretization parameter Λ and, *only in this example*, for 16 values of the twist parameter z. In all cases, we observe a spread of the position of the impurity magnetization root with respect to z. This variation decreases for smaller values of Λ and is always largest when using the discretization scheme by Žitko and Pruschke (ŽP). The spread due to z defines a magnetic field interval which, in the case of the discretization by Yoshida *et al.* (Y) and Campo and Oliveira (CO), moves towards larger fields when Λ is reduced. In contrast, the ŽP discretization leads to nested intervals so that an interval for smaller Λ is wholly contained in an interval for larger Λ. In the special case $z = 1$ (which corresponds to the smallest root), the CO and ŽP discretizations give the same result.[70] Note that the Λ dependence of the data shown in Fig. 18 is consistent with an agreement of the results of all three discretization schemes in the continuum limit $\Lambda \to 1$. However, in order to obtain reliable information about the continuum limit, it would be necessary to perform an impractical extrapolation in Λ when using the Y or CO discretizations. On the contrary, the ŽP discretization apparently allows us to make a dependable

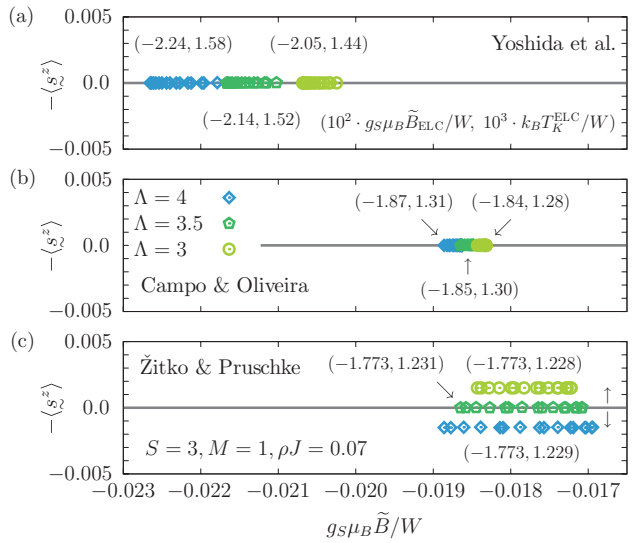

FIG. 18. (Color online) Impurity magnetization (in units of $g_S\mu_B$) for the effective Hamiltonian with $g_e = 0$ and parameters according to Eqs. (24) to (26) versus the relative magnetic field for $k_BT/W \approx 10^{-15} \approx 0$. The results have been calculated using the discretization schemes by (a) Yoshida *et al.* [with correction factor (Refs. 17,18, and 84) A_Λ] (Refs. 81–83), (b) Campo and Oliveira (Ref. 84), and (c) Žitko and Pruschke (Refs. 70 and 71). For each discretization scheme, results are presented for three values of the discretization parameter Λ and 16 values of the twist parameter z (i.e., $z_i = i/16$ with $i \in \{1,2,\ldots,16\}$). In plot (c), data points are vertically offset to enhance legibility. Numbers in parentheses denote the ELC field $\widetilde{B}_{\mathrm{ELC}}$ and the Kondo temperature T_K^{ELC} at the ELC field, respectively (cf. main text).

statement about the limit $\Lambda \to 1$ on the basis of results for only a single value of the discretization parameter: Figure 18 suggests that the continuum value of $\widetilde{B}_{\mathrm{ELC}}$ lies in the magnetic field interval that is spanned by the z-dependent roots for $\Lambda > 1$. It turns out that, using the ŽP discretization, one can obtain a better approximation for the ELC field by averaging over the z-dependent impurity magnetization roots since the resulting mean value displays only a weak dependence on Λ (cf. the numbers in parentheses in Fig. 18). The spread of the roots with respect to z then provides a safe error estimate for the mean value (amounting to a relative deviation of about 3% to 4% for $\Lambda = 3$). However, the dependence of the mean value on Λ indicates that such an error estimate is far too pessimistic. For the ŽP discretization with $\Lambda = 3$ and *four* z *values*, we expect that the relative error of the obtained ELC field $\widetilde{B}_{\mathrm{ELC}}$ is about one order of magnitude smaller than suggested by the roots' dependency on z.

Having determined $\widetilde{B}^z_{\mathrm{ELC}}$ for all values of z, we can study the thermodynamic properties of the effective model at the ELC field by calculating the impurity contribution to the entropy $S^z_{\mathrm{imp}}(T, \widetilde{B}^z_{\mathrm{ELC}})$ *for each* z *at the respective ELC field*. For thermal energies that are small compared to the bandwidth, the NRG results for $S^z_{\mathrm{imp}}(T, \widetilde{B}^z_{\mathrm{ELC}})$ can be aligned with the known universal temperature dependence of the entropy for the Kondo model with $S = \frac{1}{2}$. We find, however, that there is a dip in the entropy for thermal energies close to the band edge that becomes more pronounced for stronger scattering κ. The Kondo temperature $T_K^{\mathrm{ELC},z}$ characterizing the temperature dependence of $S^z_{\mathrm{imp}}(T, \widetilde{B}^z_{\mathrm{ELC}})$ is obtained in the following way for each value of z: By comparing with the Bethe ansatz solution for the impurity contribution to the magnetization in Sec. IV A, the value of T_K according to the definition (12) is known for the NRG results with $D = 0$ [cf. Table I and Eq. (13)]. As a first step, the result for $S^z_{\mathrm{imp}}(T, \widetilde{B}^z_{\mathrm{ELC}})$ is restricted to the linear low-temperature regime in which a continuous curve is produced using a linear fit. This fit then allows us to determine the value of $T_K^{\mathrm{ELC},z}$ by comparing with an NRG result for $S = \frac{1}{2}$ with known Kondo temperature. A better approximation for the Kondo temperature at the ELC field T_K^{ELC} is again obtained by averaging over the z-dependent values. Regarding the variation with respect to z and the error estimate for the mean value, comparable statements hold true as in the case of the ELC field.

We observe that the root of the impurity magnetization depends on temperature. This is possible since its value is apparently not determined by symmetry properties of the effective model. When the temperature exceeds the Kondo temperature at the ELC field, two effects eventually occur: The slope of the magnetization curve decreases and the root moves towards larger relative magnetic fields.

*hoeck@physik.uni-bielefeld.de
†jschnack@uni-bielefeld.de

[1] R. Sessoli, D. Gatteschi, A. Caneschi, and M. A. Novak, Nature (London) **365**, 141 (1993).
[2] D. Gatteschi, Adv. Mater. **6**, 635 (1994).
[3] C. J. Milios, A. Vinslava, W. Wernsdorfer, S. Moggach, S. Parsons, S. P. Perlepes, G. Christou, and E. K. Brechin, J. Am. Chem. Soc. **129**, 2754 (2007).
[4] L. Bogani and W. Wernsdorfer, Nat. Mater. **7**, 179 (2008).
[5] G. Rogez, B. Donnio, E. Terazzi, J.-L. Gallani, J.-P. Kappler, J.-P. Bucher, and M. Drillon, Adv. Mater. **21**, 4323 (2009).
[6] D. Gatteschi, A. Cornia, M. Mannini, and R. Sessoli, Inorg. Chem. **48**, 3408 (2009).
[7] A. Cornia, M. Mannini, P. Sainctavit, and R. Sessoli, Chem. Soc. Rev. **40**, 3076 (2011).
[8] N. Domingo, E. Bellido, and D. Ruiz-Molina, Chem. Soc. Rev. **41**, 258 (2012).
[9] D. Gatteschi, R. Sessoli, and J. Villain, *Molecular Nanomagnets* (Oxford University Press, Oxford, UK, 2006).
[10] C. Romeike, M. R. Wegewijs, W. Hofstetter, and H. Schoeller, Phys. Rev. Lett. **96**, 196601 (2006).
[11] C. Romeike, M. R. Wegewijs, W. Hofstetter, and H. Schoeller, Phys. Rev. Lett. **97**, 206601 (2006); **106**, 019902(E) (2011).
[12] D. Roosen, M. R. Wegewijs, and W. Hofstetter, Phys. Rev. Lett. **100**, 087201 (2008); **105**, 259901(E) (2010).

[13]C. F. Hirjibehedin, C.-Y. Lin, A. F. Otte, M. Ternes, C. P. Lutz, B. A. Jones, and A. J. Heinrich, Science **317**, 1199 (2007).
[14]A. F. Otte, M. Ternes, K. von Bergmann, S. Loth, H. Brune, C. P. Lutz, C. F. Hirjibehedin, and A. J. Heinrich, Nat. Phys. **4**, 847 (2008).
[15]H. Brune and P. Gambardella, Surf. Sci. **603**, 1812 (2009).
[16]K. G. Wilson, Rev. Mod. Phys. **47**, 773 (1975).
[17]H. R. Krishna-murthy, J. W. Wilkins, and K. G. Wilson, Phys. Rev. B **21**, 1003 (1980).
[18]R. Bulla, T. A. Costi, and T. Pruschke, Rev. Mod. Phys. **80**, 395 (2008).
[19]M. Mannini, F. Pineider, P. Sainctavit, L. Joly, A. Fraile-Rodriguez, M.-A. Arrio, C. C. d. Moulin, W. Wernsdorfer, A. Cornia, D. Gatteschi, and R. Sessoli, Adv. Mater. **21**, 167 (2009).
[20]M. Mannini, F. Pineider, P. Sainctavit, C. Danieli, E. Otero, C. Sciancalepore, A. M. Talarico, M.-A. Arrio, A. Cornia, D. Gatteschi, and R. Sessoli, Nat. Mater. **8**, 194 (2009).
[21]V. Corradini, F. Moro, R. Biagi, V. De Renzi, U. del Pennino, V. Bellini, S. Carretta, P. Santini, V. A. Milway, G. Timco, R. E. P. Winpenny, and M. Affronte, Phys. Rev. B **79**, 144419 (2009).
[22]S. Stepanow, J. Honolka, P. Gambardella, L. Vitali, N. Abdurakhmanova, T.-C. Tseng, S. Rauschenbach, S. L. Tait, V. Sessi, S. Klyatskaya, M. Ruben, and K. Kern, J. Am. Chem. Soc. **132**, 11900 (2010).
[23]M. Mannini, F. Pineider, C. Danieli, F. Totti, L. Sorace, P. Sainctavit, M. A. Arrio, E. Otero, L. Joly, J. C. Cezar, A. Cornia, and R. Sessoli, Nature (London) **468**, 417 (2010).
[24]R. Biagi, J. Fernandez-Rodriguez, M. Gonidec, A. Mirone, V. Corradini, F. Moro, V. De Renzi, U. del Pennino, J. C. Cezar, D. B. Amabilino, and J. Veciana, Phys. Rev. B **82**, 224406 (2010).
[25]M. Gonidec, R. Biagi, V. Corradini, F. Moro, V. De Renzi, U. del Pennino, D. Summa, L. Muccioli, C. Zannoni, D. B. Amabilino, and J. Veciana, J. Am. Chem. Soc. **133**, 6603 (2011).
[26]A. Lodi Rizzini, C. Krull, T. Balashov, J. J. Kavich, A. Mugarza, P. S. Miedema, P. K. Thakur, V. Sessi, S. Klyatskaya, M. Ruben, S. Stepanow, and P. Gambardella, Phys. Rev. Lett. **107**, 177205 (2011).
[27]V. Corradini, A. Ghirri, E. Garlatti, R. Biagi, V. De Renzi, U. del Pennino, V. Bellini, S. Carretta, P. Santini, G. Timco, R. E. P. Winpenny, and M. Affronte, Adv. Funct. Mater. **22**, 3706 (2012).
[28]C. T. Chen, Y. U. Idzerda, H.-J. Lin, N. V. Smith, G. Meigs, E. Chaban, G. H. Ho, E. Pellegrin, and F. Sette, Phys. Rev. Lett. **75**, 152 (1995).
[29]T. Funk, A. Deb, S. J. George, H. X. Wang, and S. P. Cramer, Coord. Chem. Rev. **249**, 3 (2005).
[30]M. Prinz, K. Kuepper, C. Taubitz, M. Raekers, S. Khanra, B. Biswas, T. Weyhermüller, M. Uhlarz, J. Wosnitza, J. Schnack, A. V. Postnikov, C. Schröder, S. J. George, M. Neumann, and P. Chaudhuri, Inorg. Chem. **49**, 2093 (2010).
[31]F. Meier, L. Zhou, J. Wiebe, and R. Wiesendanger, Science **320**, 82 (2008).
[32]L. Zhou, J. Wiebe, S. Lounis, E. Vedmedenko, F. Meier, S. Blügel, P. H. Dederichs, and R. Wiesendanger, Nat. Phys. **6**, 187 (2010).
[33]J. Wiebe, L. Zhou, and R. Wiesendanger, J. Phys. D: Appl. Phys. **44**, 464009 (2011).
[34]A. A. Khajetoorians, S. Lounis, B. Chilian, A. T. Costa, L. Zhou, D. L. Mills, J. Wiebe, and R. Wiesendanger, Phys. Rev. Lett. **106**, 037205 (2011).
[35]A. A. Khajetoorians, J. Wiebe, B. Chilian, S. Lounis, S. Blügel, and R. Wiesendanger, Nat. Phys. **8**, 497 (2012).
[36]C. Iacovita, M. V. Rastei, B. W. Heinrich, T. Brumme, J. Kortus, L. Limot, and J. P. Bucher, Phys. Rev. Lett. **101**, 116602 (2008).
[37]B. W. Heinrich, C. Iacovita, M. V. Rastei, L. Limot, P. A. Ignatiev, V. S. Stepanyuk, and J. P. Bucher, Eur. Phys. J. B **75**, 49 (2010).
[38]J. Brede and R. Wiesendanger, Phys. Rev. B **86**, 184423 (2012).
[39]P. E. Bloomfield, R. Hecht, and P. R. Sievert, Phys. Rev. B **2**, 3714 (1970).
[40]G. S. Poo, Phys. Rev. B **11**, 4606 (1975); **11**, 4614 (1975).
[41]V. A. Fateev and P. B. Wiegmann, Phys. Lett. A **81**, 179 (1981).
[42]N. Andrei and J. H. Lowenstein, Phys. Rev. Lett. **46**, 356 (1981).
[43]V. A. Fateev and P. B. Wiegmann, Phys. Rev. Lett. **46**, 1595 (1981).
[44]K. Furuya and J. H. Lowenstein, Phys. Rev. B **25**, 5935 (1982).
[45]V. T. Rajan, J. H. Lowenstein, and N. Andrei, Phys. Rev. Lett. **49**, 497 (1982).
[46]A. M. Tsvelick and P. B. Wiegmann, Adv. Phys. **32**, 453 (1983).
[47]N. Andrei, K. Furuya, and J. H. Lowenstein, Rev. Mod. Phys. **55**, 331 (1983).
[48]P. Schlottmann, Z. Phys. B: Condens. Matter **51**, 223 (1983).
[49]J. H. Lowenstein, Phys. Rev. B **29**, 4120 (1984).
[50]A. M. Tsvelick and P. B. Wiegmann, J. Stat. Phys. **38**, 125 (1985).
[51]P. D. Sacramento and P. Schlottmann, Phys. Rev. B **40**, 431 (1989).
[52]K. Takegahara and T. Kasuya, Phys. B (Amsterdam) **163**, 216 (1990).
[53]A. C. Hewson, J. Bauer, and W. Koller, Phys. Rev. B **73**, 045117 (2006).
[54]C. J. Wright, M. R. Galpin, and D. E. Logan, Phys. Rev. B **84**, 115308 (2011).
[55]R. Žitko, in *Physical Properties of Nanosystems*, edited by J. Bonča and S. Kruchinin (Springer, Dordrecht, 2011), pp. 247–257.
[56]A. Hackl, M. Vojta, and S. Kehrein, Phys. Rev. B **80**, 195117 (2009).
[57]P. Fritsch and S. Kehrein, Phys. Rev. B **81**, 035113 (2010).
[58]M. Schiró, Phys. Rev. B **81**, 085126 (2010).
[59]M. Pletyukhov, D. Schuricht, and H. Schoeller, Phys. Rev. Lett. **104**, 106801 (2010).
[60]M. Heyl and S. Kehrein, J. Phys.: Condens. Matter **22**, 345604 (2010).
[61]F. B. Anders and A. Schiller, Phys. Rev. Lett. **95**, 196801 (2005); Phys. Rev. B **74**, 245113 (2006).
[62]A. Hackl, D. Roosen, S. Kehrein, and W. Hofstetter, Phys. Rev. Lett. **102**, 196601 (2009).
[63]R. Žitko, R. Peters, and T. Pruschke, Phys. Rev. B **78**, 224404 (2008).
[64]R. Žitko, R. Peters, and T. Pruschke, New J. Phys. **11**, 053003 (2009).
[65]R. Žitko and T. Pruschke, New J. Phys. **12**, 063040 (2010).
[66]A. Bencini and D. Gatteschi, *Electron Paramagnetic Resonance of Exchange Coupled Systems* (Springer, Berlin, 1990).
[67]I. Affleck, A. W. W. Ludwig, and B. A. Jones, Phys. Rev. B **52**, 9528 (1995).
[68]A. Schiller and L. De Leo, Phys. Rev. B **77**, 075114 (2008).
[69]T. Costi, in *Density-Matrix Renormalization–A New Numerical Method in Physics*, edited by I. Peschel, M. Kaulke, X. Wang, and K. Hallberg, Lecture Notes in Physics, Vol. 528 (Springer, Berlin, 1999), pp. 3–25.
[70]R. Žitko and T. Pruschke, Phys. Rev. B **79**, 085106 (2009).
[71]R. Žitko, Comput. Phys. Commun. **180**, 1271 (2009).

[72] A. C. Hewson, *The Kondo Problem to Heavy Fermions* (Cambridge University Press, Cambridge, 1993).

[73] In order to calculate $M_{\rm imp}(x, T = 0)/g_S\mu_B$ for magnetic fields $g_S\mu_B B \geqslant k_B T_H$, we have employed Eq. (5.1.35) of Ref. 46 for all considered values of S. In the regime $g_S\mu_B B < k_B T_H$, Eq. (5.1.37) of Ref. 46 with an additional factor $\frac{1}{4}$ has been used for $S = \frac{1}{2}$ and Eq. (33) of Ref. 41 for $S \geqslant 1$, respectively. We suspect that the latter equation ought to read as [cf. Eq. (5.1.38) of Ref. 46]

$$\frac{M_{\rm imp}(x)}{g_S\mu_B} = S - 1/2 + \frac{1}{2\pi^{3/2}}\int_0^\infty d\omega\Bigg(\frac{\sin(2\pi\omega(S-1/2))}{\omega} \times \Gamma(1/2-\omega)\mathrm{e}^{-2\omega|\ln(g_S\mu_B B/k_B T_H)|}(\omega/\mathrm{e})^\omega\Bigg) + \frac{1}{2}\sum_{n=0}^{\infty}\ldots.$$

For integer impurity spin S (in which case the maxima and minima of the sine coincide with the poles of the gamma function in the integrand), we have been unable to obtain converged results for the above integral in the field regime $g_S\mu_B B \lesssim k_B T_H$. For this reason, part of the BA curve is missing in Fig. 1(b).

[74] It might seem more natural to compare with the easily obtainable magnetization of a free spin. However, we observe that for the chosen value of Λ and zero coupling NRG is apparently not able to fully reproduce the finite-temperature behavior of a free spin. For this reason, we rather use NRG results with $J = 0$ for the comparison.

[75] D. C. Mattis, Phys. Rev. Lett. **19**, 1478 (1967).

[76] D. M. Cragg and P. Lloyd, J. Phys. C: Solid State Phys. **12**, L215 (1979).

[77] H.-U. Desgranges and K. D. Schotte, Phys. Lett. A **91**, 240 (1982).

[78] L. Merker, A. Weichselbaum, and T. A. Costi, Phys. Rev. B **86**, 075153 (2012).

[79] H. R. Krishna-murthy, J. W. Wilkins, and K. G. Wilson, Phys. Rev. B **21**, 1044 (1980).

[80] It seems permissible to use the effective model for $g_e = 0$ as a *guide* for the interpretation of the results in Fig. 9 since we are primarily interested in the behavior of the impurity magnetization $\mathcal{M}$ whose dependence on g_e we know. As demonstrated in Appendix C for not too large D, $\mathcal{M}$ is proportional to $M_{\rm imp}$ for equal g factors and fixed coupling strength, and a reduction of g_e effectively rescales the magnetic field argument of $\mathcal{M}$. This of course changes the ELC field, but preserves the shape of the impurity magnetization curve (cf. Fig. 16).

[81] M. Yoshida, M. A. Whitaker, and L. N. Oliveira, Phys. Rev. B **41**, 9403 (1990).

[82] W. C. Oliveira and L. N. Oliveira, Phys. Rev. B **49**, 11986 (1994).

[83] S. C. Costa, C. A. Paula, V. L. Líbero, and L. N. Oliveira, Phys. Rev. B **55**, 30 (1997).

[84] V. L. Campo and L. N. Oliveira, Phys. Rev. B **72**, 104432 (2005).

[85] However, while being nonperturbative in J, NRG still relies on a discretization of the electronic degrees of freedom. For $\rho J > 0.4$ we observe artifacts in the NRG results: $M_{\rm imp}$ becomes negative for $S = \frac{1}{2}$, whereas $M_{\rm imp}(\rho J)$ curves for different magnetic fields eventually cross for $S \geqslant 1$. In contrast, the impurity magnetization $\mathcal{M}$ does not display any obvious anomalies. Figures 14 and 15 are basically unaffected by the aforementioned problems.

[86] G. Zaránd, T. Costi, A. Jerez, and N. Andrei, Phys. Rev. B **65**, 134416 (2002).

[87] P. B. Vigman and A. M. Finkel'shteĭn, Zh. Eksp. Teor. Fiz. **75**, 204 (1978) [Sov. Phys. JETP **48**, 102 (1978)].

[88] T. A. Costi and G. Zaránd, Phys. Rev. B **59**, 12398 (1999).